the Energy to Lead

FINAL REPORT

GTI PROJECT NUMBER 20835.1.66

PE 4710 Mitered Elbow Finite Element Analysis

Date Submitted: April 5, 2016

Revised: April 11, 2016

Project Investors:
PPI

GTI Project Manager:
Natalya Bates
Project Manager
847-768-0953
natalya.bates@gastechnology.org

GTI Principal Investigators:
Ernest Lever
Senior Institute Engineer
847-768-3415
ernest.lever@gastechnology.org

Oren Lever
Principal Engineer
847-768-0668
oren.lever@gastechnology.org

Gas Technology Institute
1700 S. Mount Prospect Rd.
Des Plaines, Illinois 60018
www.gastechnology.org

Legal Notice

This information was prepared by Gas Technology Institute ("GTI") for Plastics Pipe Institute (PPI).

Neither GTI, the members of GTI, the Sponsor(s), nor any person acting on behalf of any of them:

a. Makes any warranty or representation, express or implied with respect to the accuracy, completeness, or usefulness of the information contained in this report, or that the use of any information, apparatus, method, or process disclosed in this report may not infringe privately-owned rights. Inasmuch as this project is experimental in nature, the technical information, results, or conclusions cannot be predicted. Conclusions and analysis of results by GTI represent GTI's opinion based on inferences from measurements and empirical relationships, which inferences and assumptions are not infallible, and with respect to which competent specialists may differ.

b. Assumes any liability with respect to the use of, or for any and all damages resulting from the use of, any information, apparatus, method, or process disclosed in this report; any other use of, or reliance on, this report by any third party is at the third party's sole risk.

c. The results within this report relate only to the items tested

Table of Contents

Table of Figures

List of Tables

List of Acronyms

ASTM	American Society for Testing and Materials
BRF	Bend Radius Factor (*BRF x OD = Bend Radius*)
CAD	Computer Aided Design
DoE	Design of Experiment
FEA	Finite Element Analysis
FEM	Finite Element Method
GTI	Gas Technology Institute
HDPE	High Density Polyethylene
ID	Inner Diameter
OD	Outer Diameter
PPI	Plastics Pipe Institute
RSM	Response Surface Methodology
SDR	Standard Dimension Ratio
GSR	Geometric Strength Ratio
DR	Dimension Ratio

Executive Summary

A series of 357 nonlinear finite element analyses was conducted to evaluate the performance of various configurations of fabricated PE 4710 elbows.

In order to understand how a particular design behaves it is necessary to conduct a large number of analyses that capture the range of boundary conditions and material properties. The approach taken in the study was to use a "Virtual" Design of Experiment (DoE). In this approach each Finite Element Analysis (FEA) is viewed as a virtual experiment.

Preliminary analysis showed that the following six input parameters are sufficient to fully understand the performance characteristics of a mitered elbow:

1. Dimension Ratio - *DR*
2. Miter Angle - *Angle*
3. GSR - *GSR*
4. Bend Radius Factor – *BRF*
5. Ambient Temperature - *Temperature*
6. Operating Pressure - *Pressure*

A face centered cubic response surface design was chosen. Fifty (50) design points would be sufficient to fully resolve all second-order interactions of input parameters. An additional 27 design points were added to augment the design.

A high-quality response surface model was achieved with low standard error that is capable of properly analyzing all of the input FEA results. **Appendix 0** presents the initial model information prior to actual analysis of the results that are presented in detail in **Appendices 1 through 16**. In **Appendix 17** we present the stress strain curves on which the analyses were based and define the stress ratio that is used in several of the analyses.

Temperature dependent material properties were used to assess the impact of ambient temperature on elbow performance. The material model used reflects the stresses developed in an elbow upon pressurization and does not include creep of the material. This level of analysis is sufficient as the Hydrostatic Design Stress (HDS) of the material accounts for long term creep effects for calculated stresses equal to, or lower than the HDS. The stress-strain curves were developed by detailed testing of physical test specimens of a typical PE 4710 material provided by a leading resin manufacturer.

Four arcs shown in **Figure 8** were chosen to fully describe the stress state of each elbow configuration. Response surfaces were developed for the average stress among each of these arcs, the maximum stress among each of these arcs, and the ratio of each of these stresses to the temperature dependent yield stress of the material.

The first principal stress P1 is a good indicator of the stress state of the fabricated elbow under all loading conditions for all fitting configurations. The highest stresses occur at the intrados of the miter joint; hence the first principle stress (hoop stress) at this location was used in all calculations in the report. The design criterion chosen in this report is the average of the first principle stresses radially across the intrados wall thickness (see "intrados" line in **Figure 8**). When this average is at or below the pipe hoop stress the design is considered acceptable regardless of peak stresses along this line that may be higher than the pipe hoop stress.

The effect of fusion beads on the stress fields in the miter joint were evaluated and found to be insignificant. Therefore, to avoid unnecessary modeling complexity, the full analysis did not include fusion beads in the geometry of the elbow.

Internally and externally reinforced designs were compared and found to be equivalent. Only externally reinforced elbows were modeled in the full analysis.

Analyses were run to verify that the elbow stresses for DR based designs are insensitive to pipe diameter. The results differed by less than one half of a percent across all configurations and diameters thus justifying the modeling of configurations for a single pipe size.

The impact of mesh size on the stress results was investigated. The mesh size was chosen to minimize analysis time without compromising the stress result. The stress results differed by less than one tenth of a percent from FEA models with a high resolution mesh.

The analysis presented in this report justify the use of ASME B31.3-2012 Section 304.2.3 equation 4a (**Equation 1** in this study) as the basis for PE 4710 mitered elbow design. This equation[1] can be manipulated to produce:

$$t = t_0\left(1 + 0.3073\sqrt{\frac{r_2}{t}}\tan\theta\right) \qquad \textbf{Equation 7}$$

t pressure design thickness
t_0 nominal pipe wall thickness
r_2 mean radius of pipe
θ Miter cut angle

1 Full derivation of equations is shown starting on page 42.

Equation 7 is in turn manipulated to produce:

$$\mathrm{GSR} = \frac{1}{1+0.3073\sqrt{\frac{r_2}{t}}\tan\theta} \qquad \textbf{Equation 9}$$

Equation 7 or **Equation 9** is all the elbow designer needs to determine the nominal increase in wall thickness needed for an HDPE mitered elbow.

Using these two equations we show that the current industry practice of using a DR of one standard dimension less than the pipe for the fabricated elbow, which results in an approximately 25% increase in wall thickness, is a very reasonable approach and is nominally conservative up to a miter cut of 15° and for DRs less than or equal to 19. For a miter cut of 22.5° the approach is nominally conservative for DR 7.

The effect of the Bend Radius was found to have insignificant effect on the stress at the intrados. However, as the bend radius decreases the stress fields of the pipe and intrados move closer to one another and fully merge at BRF = 1. The average stress between the pipe and intrados is higher than the pipe hoop stress for this configuration.

The Response Surface Methodology (RSM) presented in the appendices of this report can be used to take into account more complex sets of design constraints for specific application scenarios.

Parametric Geometry Model

A Computer-Aided Design (CAD) model was created based on a draft ASTM specification that is being prepared by a task group of the Plastics Pipe Institute.

The model was constructed parametrically to allow it to accommodate all possible configurations under the draft standard and was driven by design tables that allowed for quick configuration additions.

Butt-fusion beads were modeled in a single configuration to assess their impact on the local and global stress fields. The results of this sub analysis are presented in the section **Fusion Beads**. The net effect of the beads on the stress fields is shown in **Figure 31** through **Figure 33**. It can be seen that the effect is minor and it was decided not to model them in all configurations under the scope of this project due to their complex and inconsistent geometry, which presented major difficulties in including them in a DoE.

The analyses in this project follow up on the previous project, where a BRF of 2.5 was evaluated. The following BRFs: 2, 1.5, 1, and 0.75 were added to the analysis.

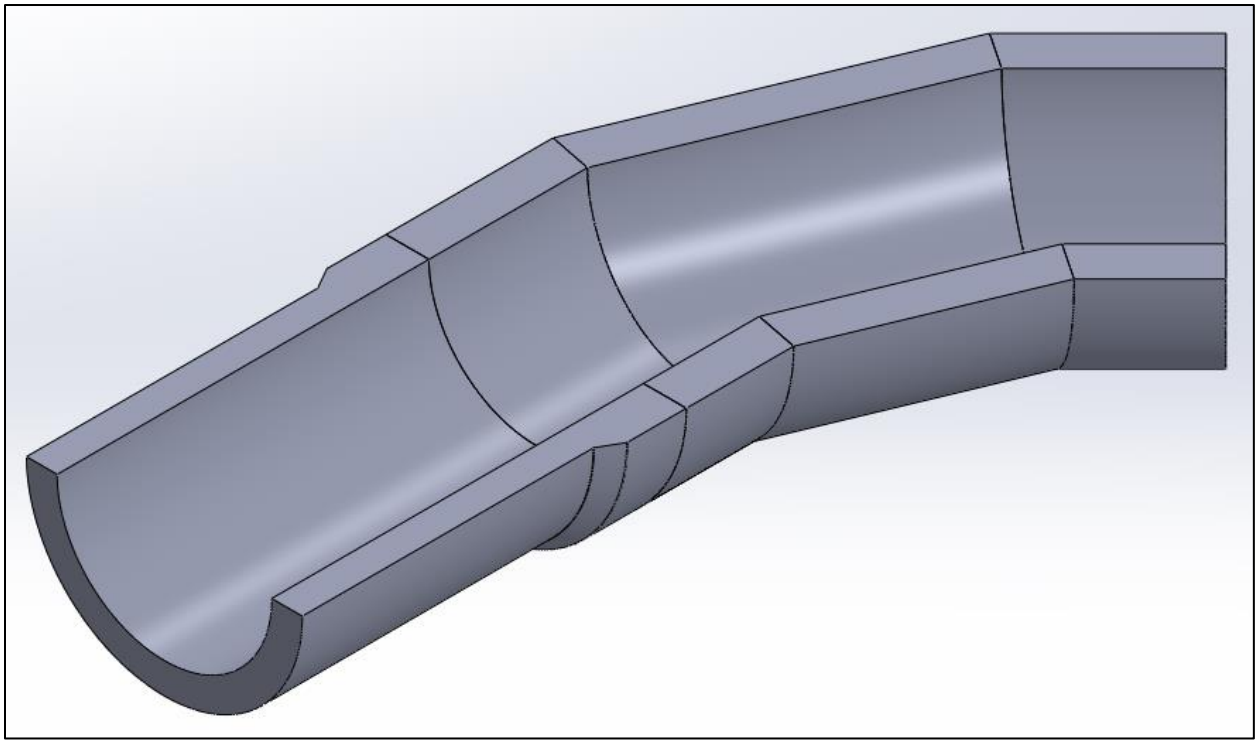

Figure 1. Quarter model of 90°, constant ID, 5-segment miter-bend for FEA

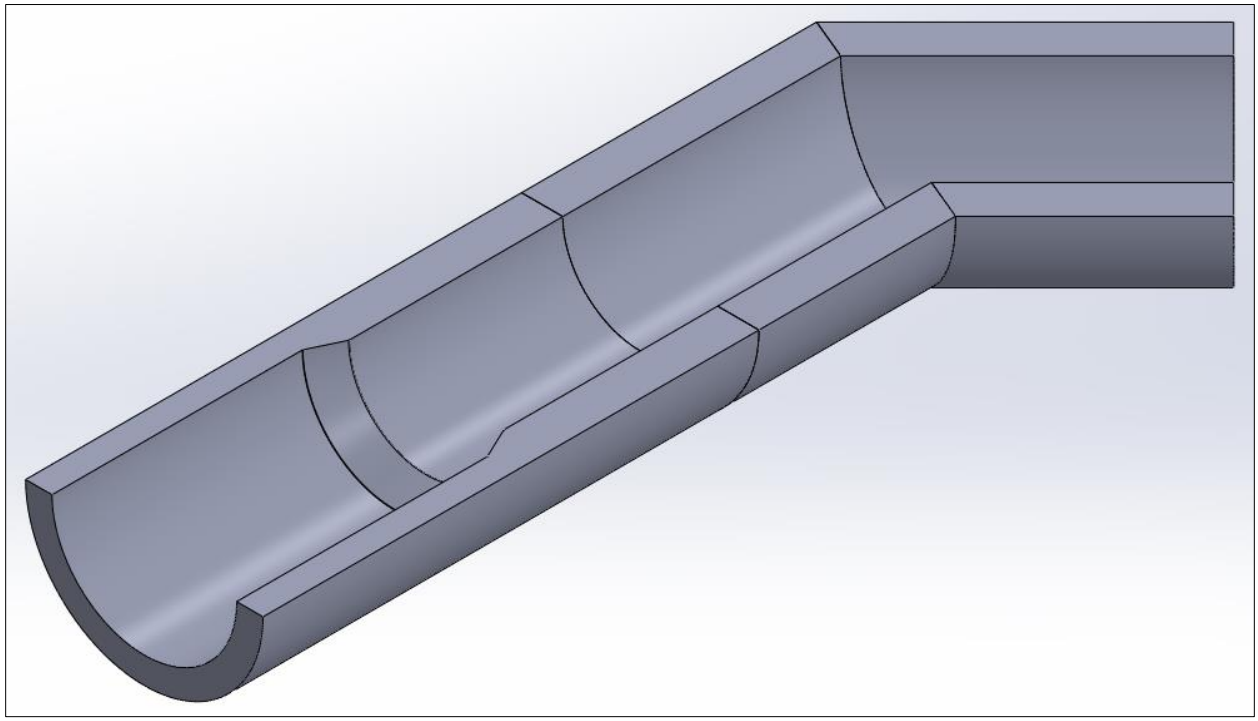

Figure 2. Quarter model of 90°, constant OD, 3-segment miter-bend for FEA

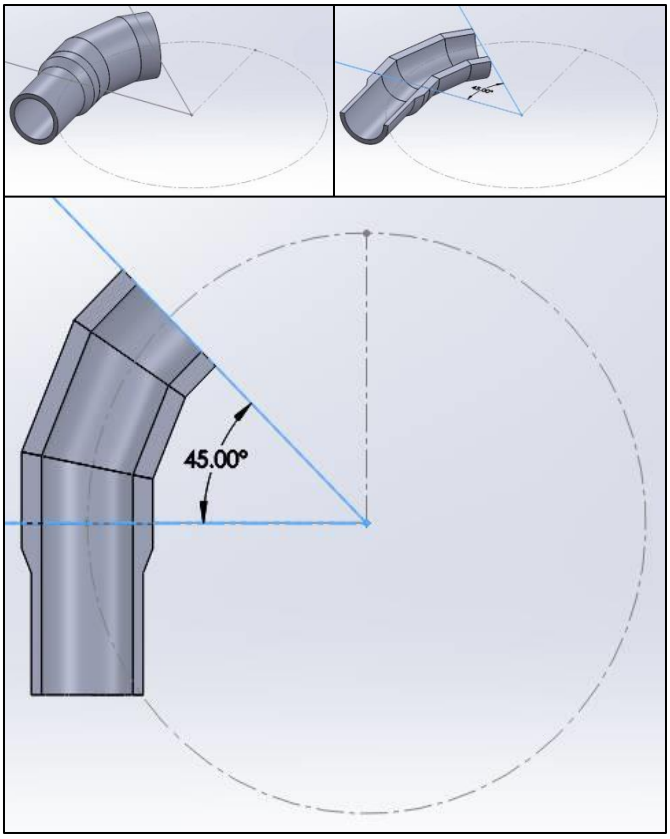

Figure 3. Quarter model configuration

Finite Element Analysis Model

The FEA used a 90°, constant ID miter bend for all simulations. A quarter model was used in order to reduce computation time. The simulation assumed symmetry in all directions (see **Figure 4**) meaning that, as pressure was applied, the elbow was free to expand (hoop) and to move in the radial direction of the bend radius. The elbow's end was not otherwise constrained. Defining symmetry in all directions constituted the simplest loading condition where no secondary bending moments are introduced.

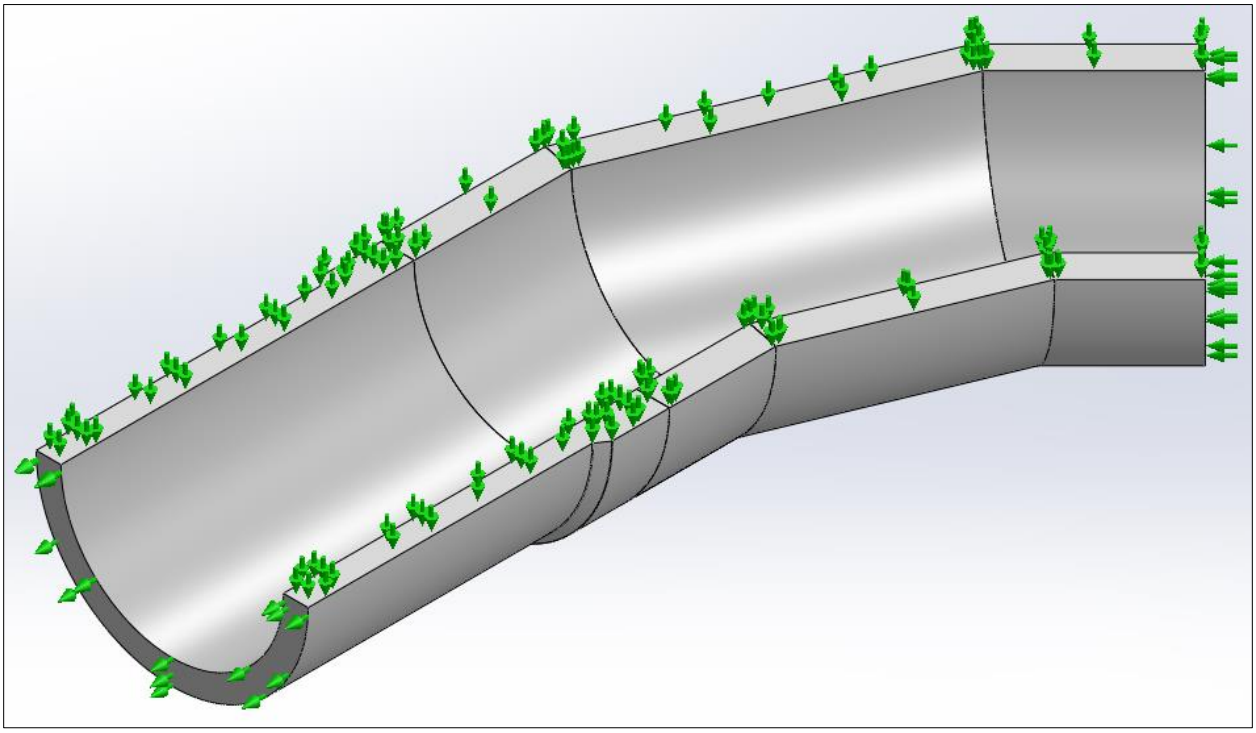

Figure 4. Symmetry surfaces

Pressure was applied to all internal surfaces (**Figure 5**). Mesh element size was adjusted for each geometric configuration such that the nominal pipe wall had one element across its thickness and the joints had five; see **Figure 6** and **Figure 7**, respectively. The elements were second order elements that maintained a good balance of accuracy and computation time. **Figure 8** shows the locations where stresses were probed.

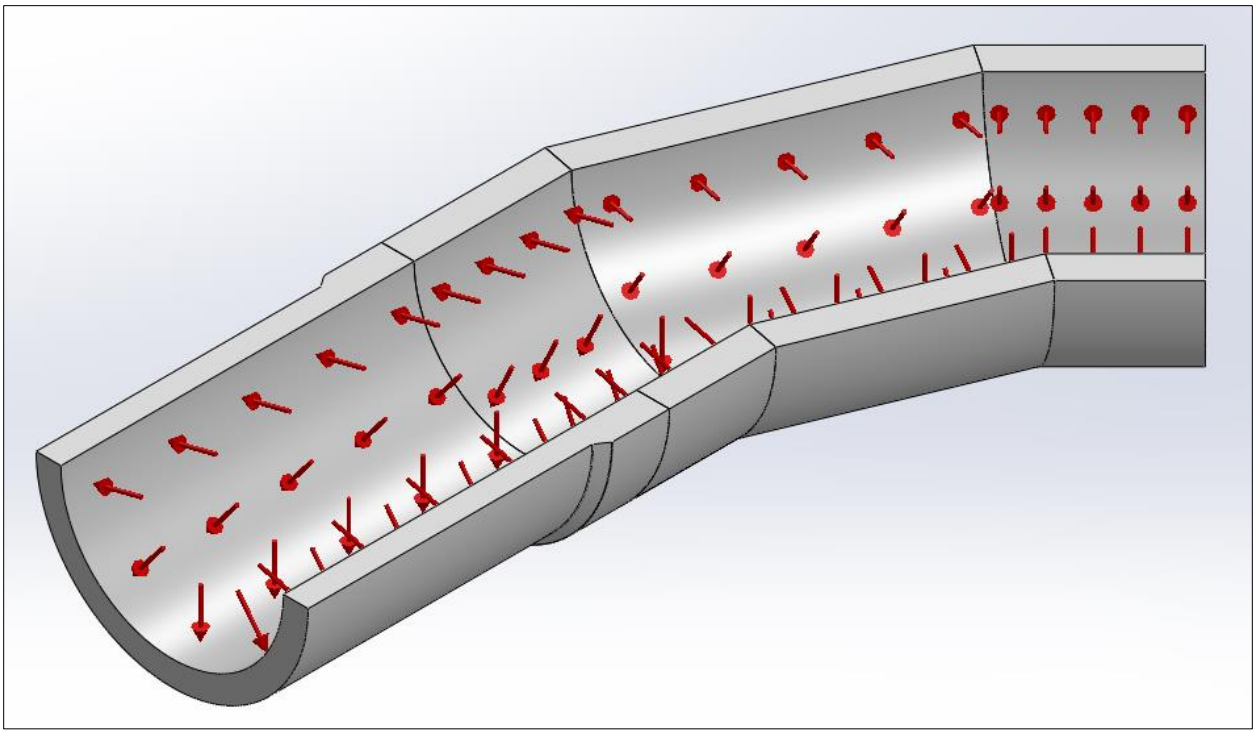

Figure 5. Pressure surfaces

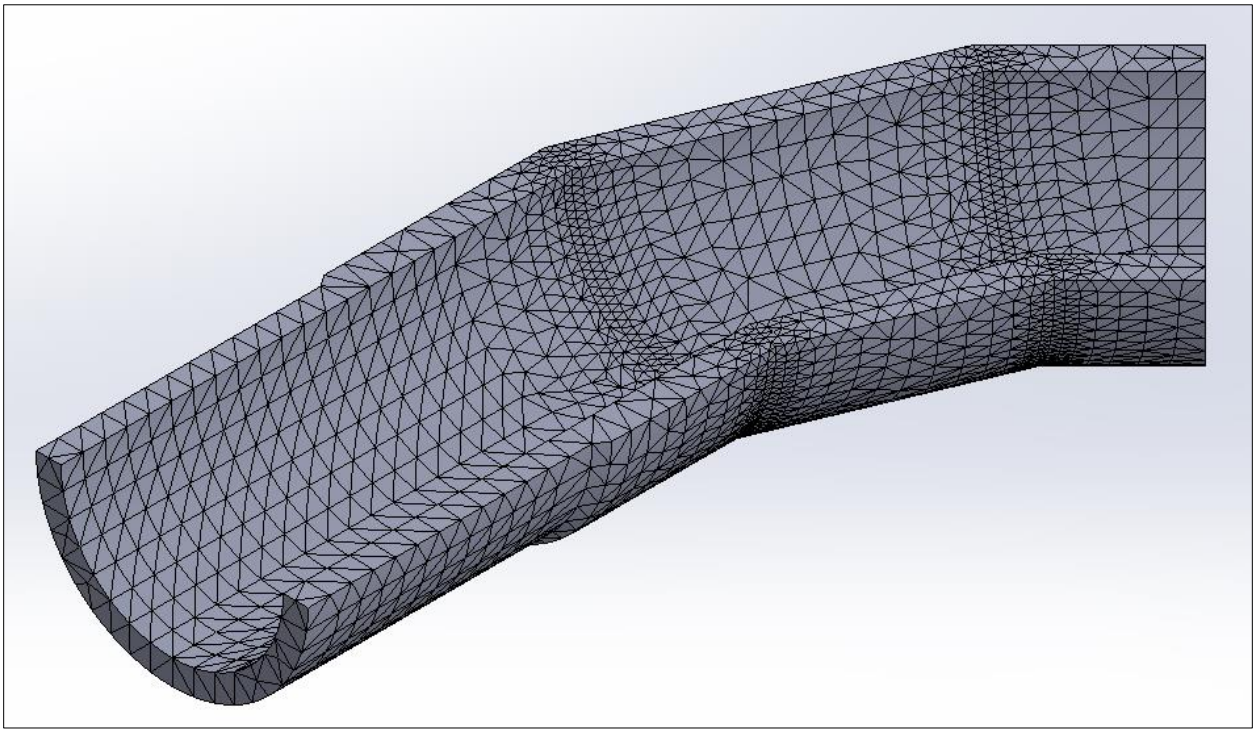

Figure 6. Typical mesh

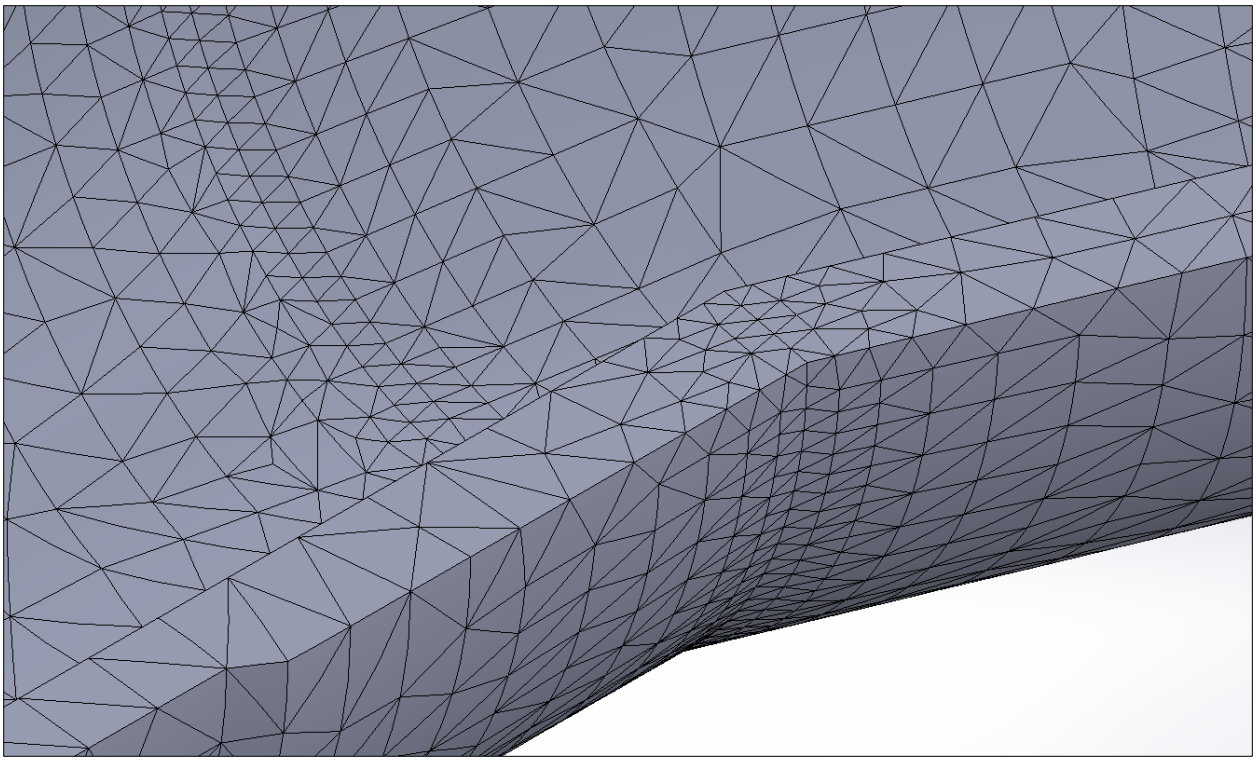

Figure 7. Typical mesh, joint detail

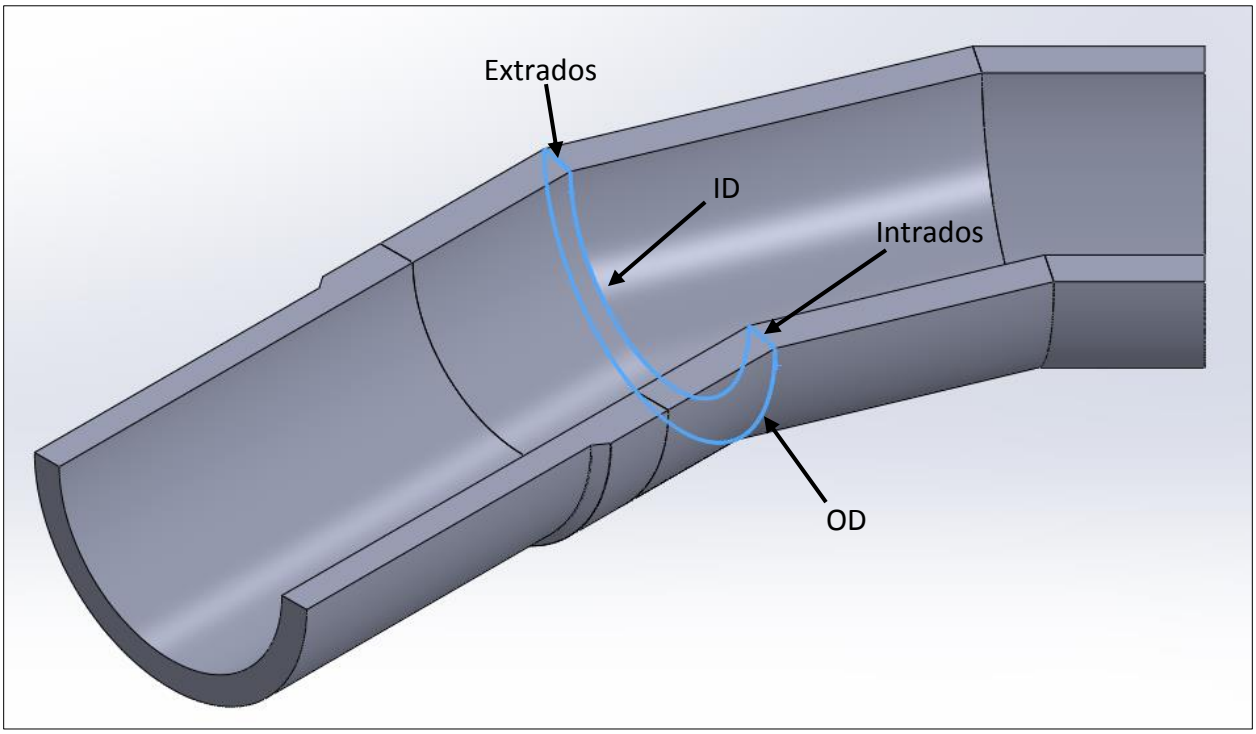

Figure 8. Probe locations

Material Constitutive Model

FEA used a nonlinear elastic material model based on HDPE tensile stress-strain curves at 0°C (32°F), 20°C (68°F), and 40°C (104°F) temperatures, all pulled at 0.001/s engineering strain rate. The low strain rate was chosen to more closely simulate actual pressurization rates. The model can be considered valid within the temperature range 32°F – 104°F.

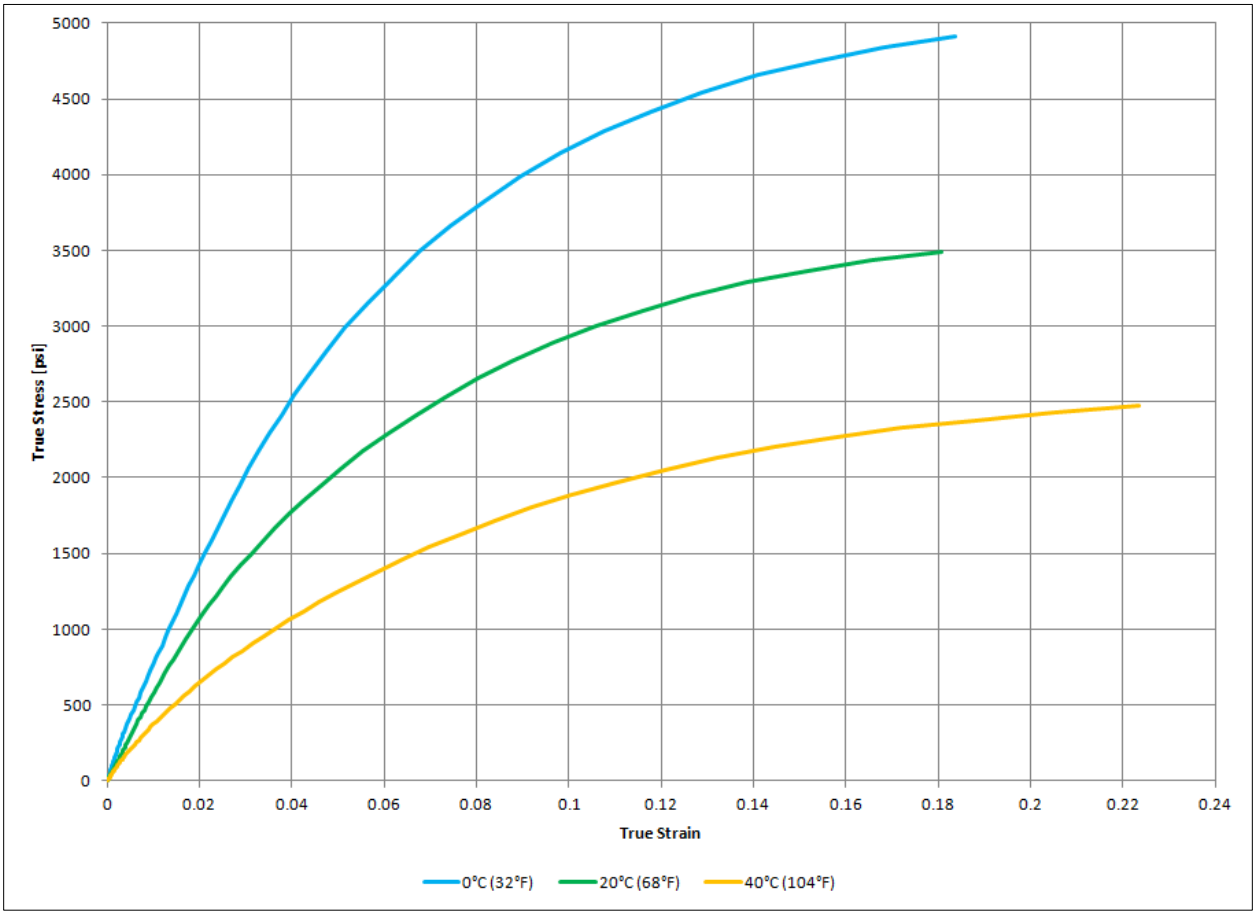

Figure 9. HDPE stress-strain curves, 0.001/s engineering strain rate

The nonlinear elastic model did not account for material relaxation or creep and, therefore, the results of the FEA represent an estimation of the immediate stresses upon pressurization. This approach is conservative as stress relaxation is not accounted for. Poisson's ratio was set at 0.41.

Significance of Pipe Diameter

The analysis results of the first set of tests (**Table 1**) show that pipe diameter has no effect on the stresses due to the absence of secondary bending moments. Stresses are dependent on pipe dimension ratio and applied pressure, therefore, for example, a 34" SDR 11 pipe with a 3xOD miter bend will have the same stress as a 14" SDR 11 pipe with a 3xOD miter bend.

Table 1. Average hoop stress (psi) at miter joint, SDR 17, Gore-DR 13.6 (Pipe DR 17 * GSR 0.8), 125 psig, 68°F

Size	5-segment	4-segment	3-segment
14" IPS	962.4	1054.1	1230.9
34" IPS	968.0	1056.2	1232.0
Difference	0.58%	0.20%	0.09%

When the pipeline design is based on the DR of the pipe, stresses in an unrestrained miter elbow have no dependence on pipe diameter, therefore the subsequent DoE matrix did not have diameter as a variable in order to reduce the number of analyses.

Comparison of Internally and Externally Reinforced Elbow Stresses

The average first principal stress at the intrados was evaluated for 14" IPS DR 11 with BRF=2.5 at two extreme configurations; heavy wall five segment and thin wall three segment elbows for both the ID reinforced and OD reinforced designs. There is less than 1% difference in the results, therefore only OD reinforced elbows were considered in the FEA study.

Table 2. Comparison of stresses in ID and OD reinforced mitered elbows

Diameter Control	Configuration	Pressure (psig)	Intrados P1 Avg. (psi)	Extrados P1 Avg. (psi)
OD reinforced	14IPS11-5-06-20C	250	736.04	447.93
OD reinforced	14IPS11-3-08-20C	250	1358.4	521.11
ID reinforced	14IPS11-5-06-20C	250	729.11	449.37
ID reinforced	14IPS11-3-08-20C	250	1349.5	492.66
ID/OD	14IPS11-5-06-20C	NA	0.991	1.003
ID/OD	14IPS11-3-08-20C	NA	0.993	0.945

NA: Not Applicable

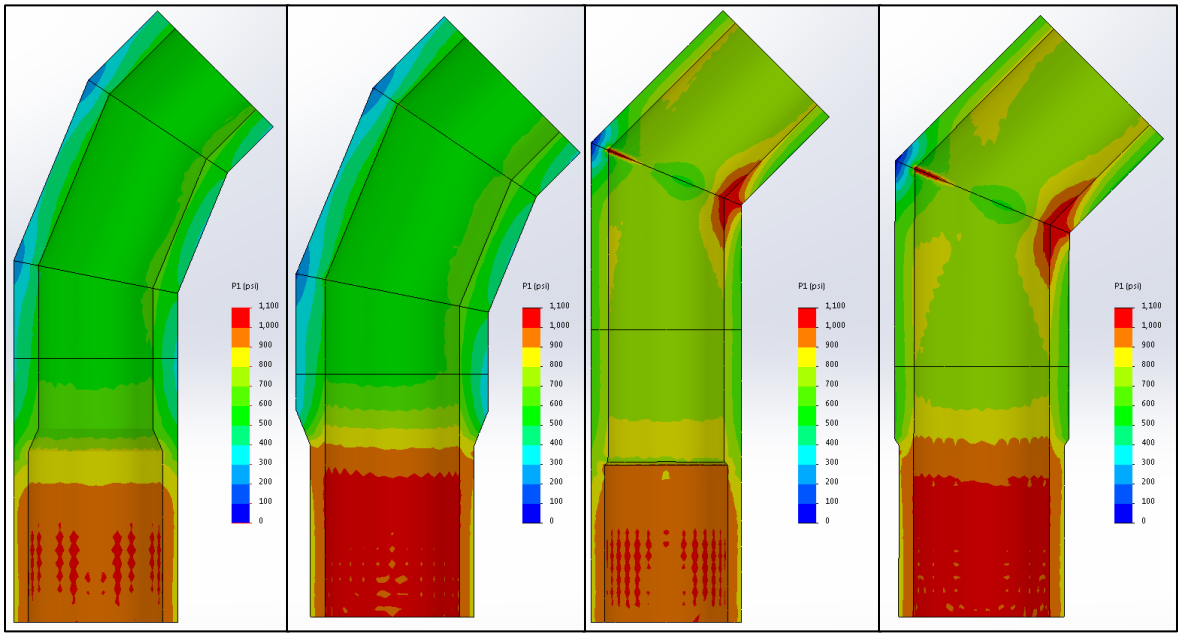

Figure 10. Comparison of stresses in ID and OD reinforced elbows

To further illustrate the similarity between externally and internally reinforced elbows, **Figure 11** through **Figure 14** compare internal reinforcement to external reinforcement in terms of different stress measures. The figures show data points from BRF=1.5 and BRF=1.0 configurations. For each data point on the figures, the horizontal axis value represents the externally reinforced configuration and the vertical axis value represents the otherwise identical internally reinforced configuration. If both values are identical, the data point will fall on the equivalence line.

Figure 11 compares reinforcement configurations in terms of the maximum von Mises stress at the intrados. The stress difference between internal and external reinforcement is within ±5% in all cases.

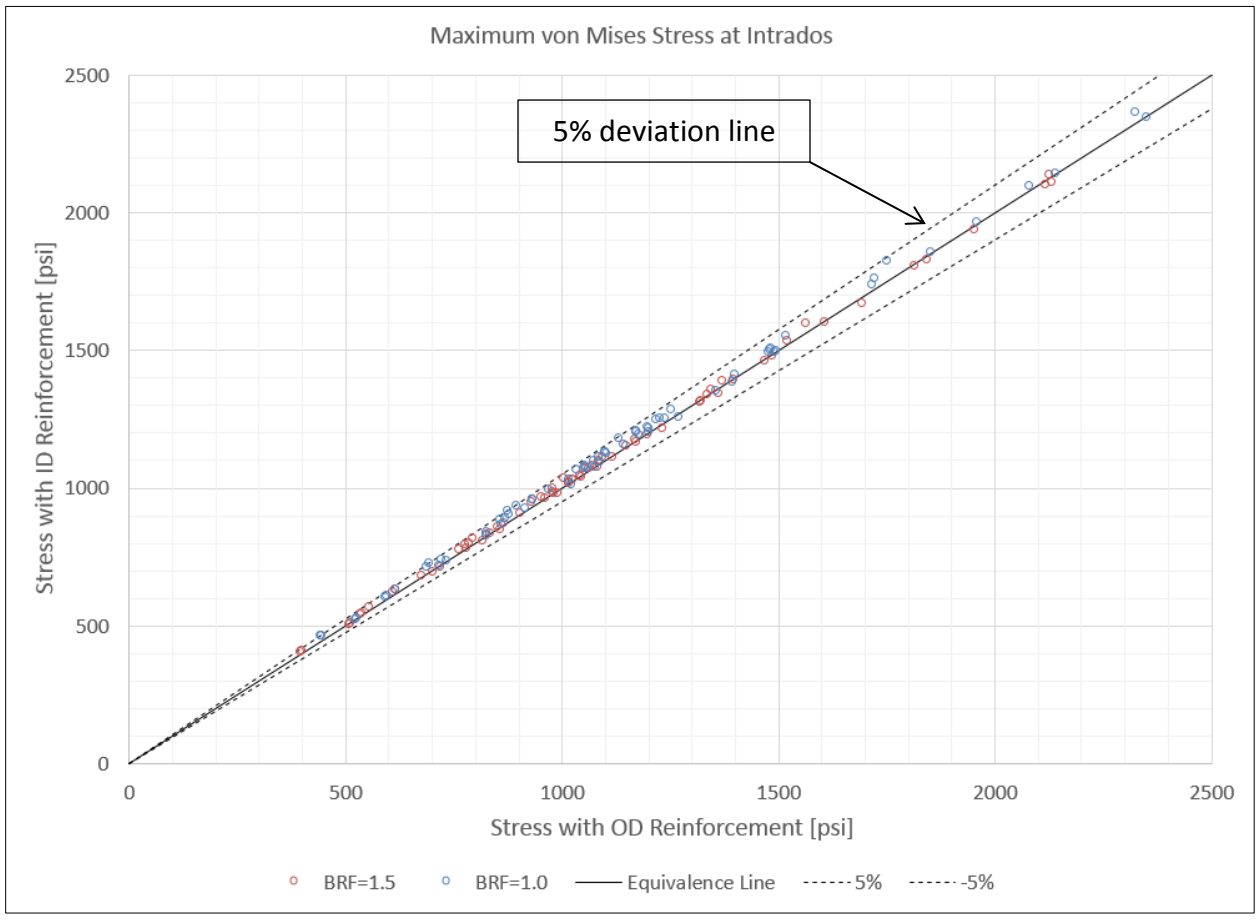

Figure 11. Comparison of OD and ID reinforced elbows, by maximum von Mises stress at intrados

Figure 12 compares reinforcement configurations in terms of the maximum first principal stress at the intrados. The stress difference between internal and external reinforcement is also within 5% in all cases.

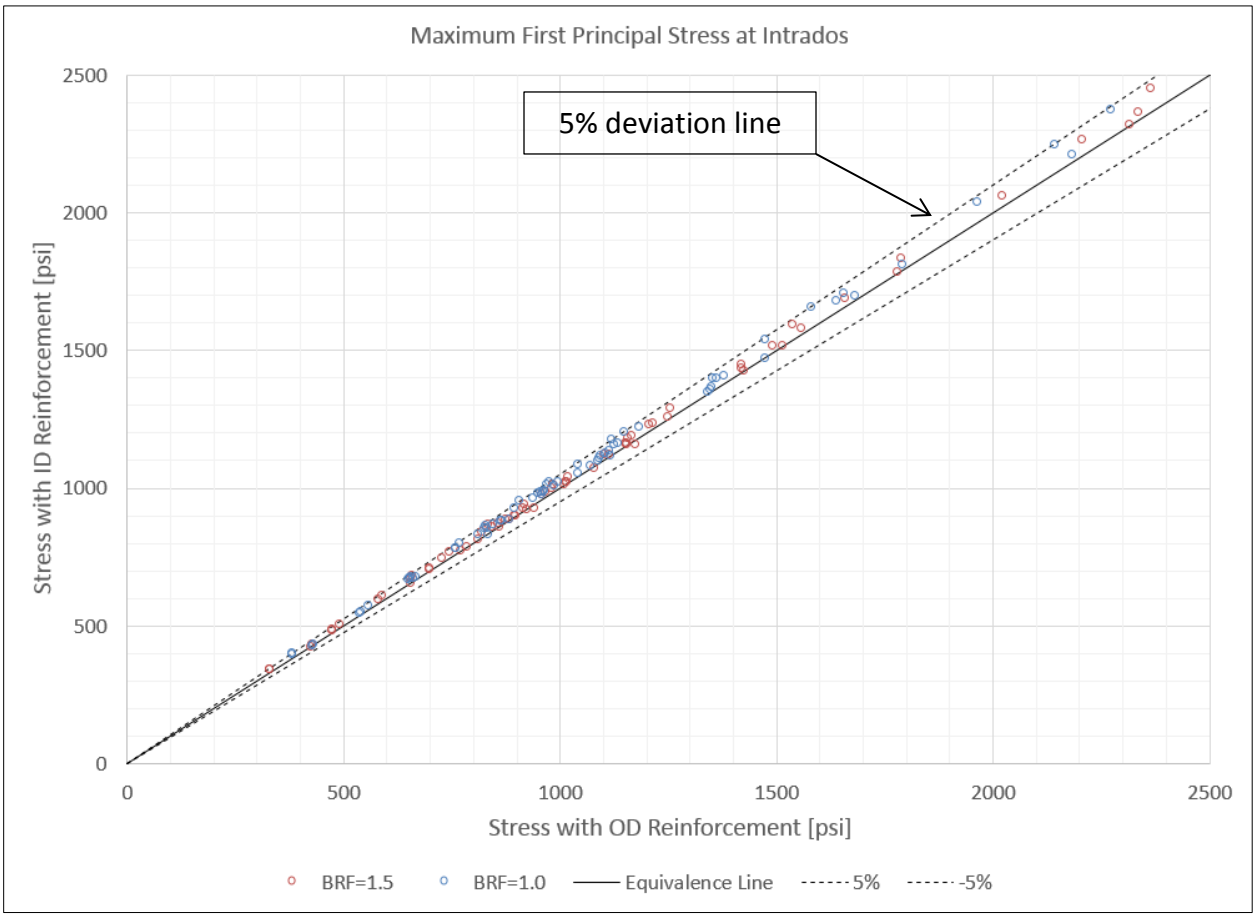

Figure 12. Comparison of OD and ID reinforced elbows, by maximum first principal stress at intrados

Figure 13 compares reinforcement configurations in terms of the average von Mises stress at the intrados. The stress difference between internal and external reinforcement is within ±5% in all cases.

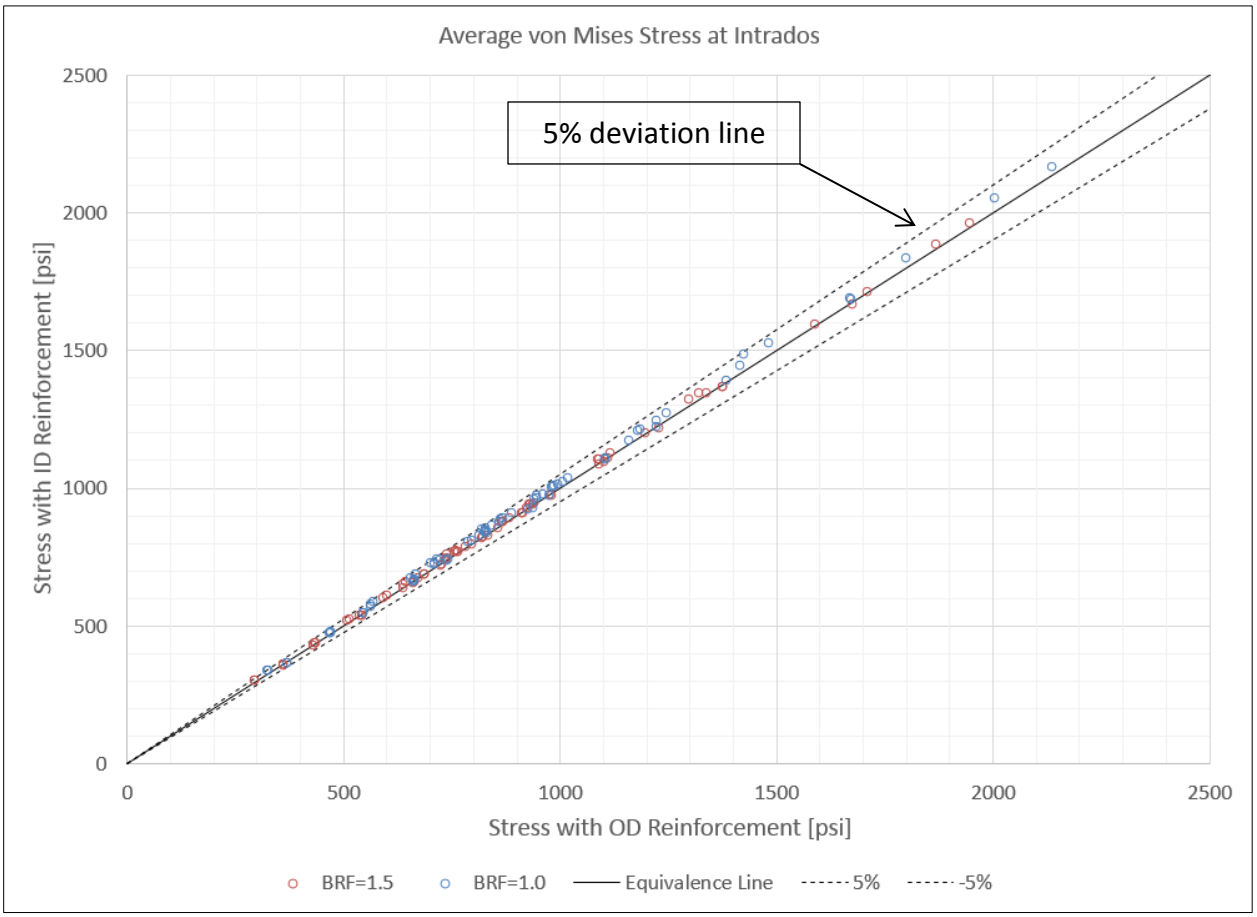

Figure 13. Comparison of OD and ID reinforced elbows, by average von Mises stress at intrados

Figure 14 compares reinforcement configurations in terms of the average first principal stress at the intrados. The stress difference between internal and external reinforcement is within ±5% in all cases.

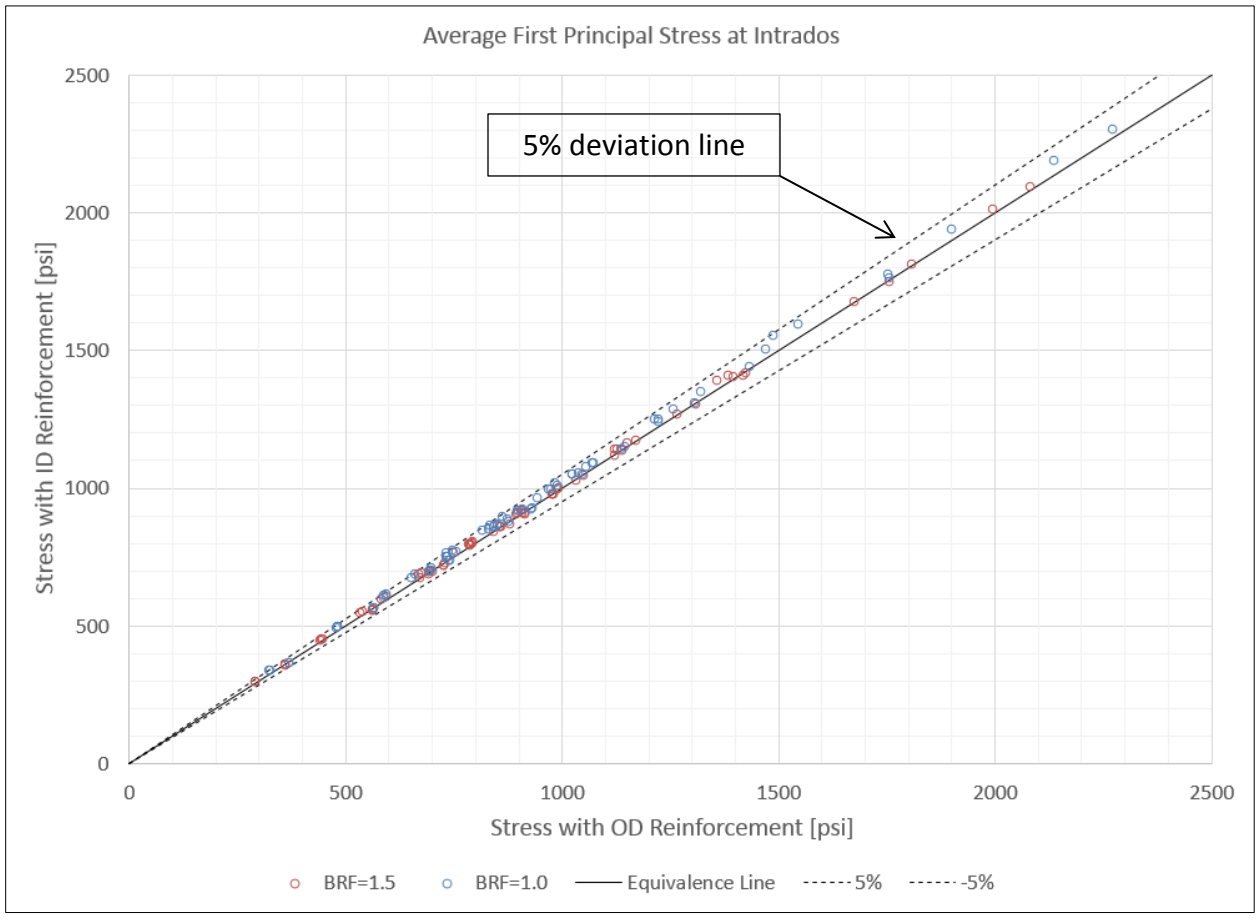

Figure 14. Comparison of OD and ID reinforced elbows, by average first principal stress at intrados

Of minor note is that, as seen in the comparison figures above, in the case of BRF=1.0 the internally reinforced configurations have a slightly higher stress deviation than in the BRF=1.5 case. This means that at larger BRF values the stresses of OD and ID reinforced elbows can be considered equivalent.

In the case of BRF=1.0, the analysis data shows that the stress difference between internal and external reinforcement of an elbow is within 5%, with external reinforcement having slightly lower stresses.

Design of Experiment

In order to determine the influence of the various geometry and boundary condition variables on stresses in the elbows, DoE and RSM were employed. Using these techniques, an appropriate FEA test matrix was developed and the influences of the test variables could be resolved.
Analyses were carried out to analyze the effects of bend radius OD-factor, pipe DR, joint angle, elbow DR factor, temperature, and pressure.

FEA Results

The following figures show typical stress plots from the DoE analyses. **Figure 15** shows the quarter model of a 14" IPS, SDR 11, BRF=2.5, 3-segment miter elbow at 200 psig, at 32°F.

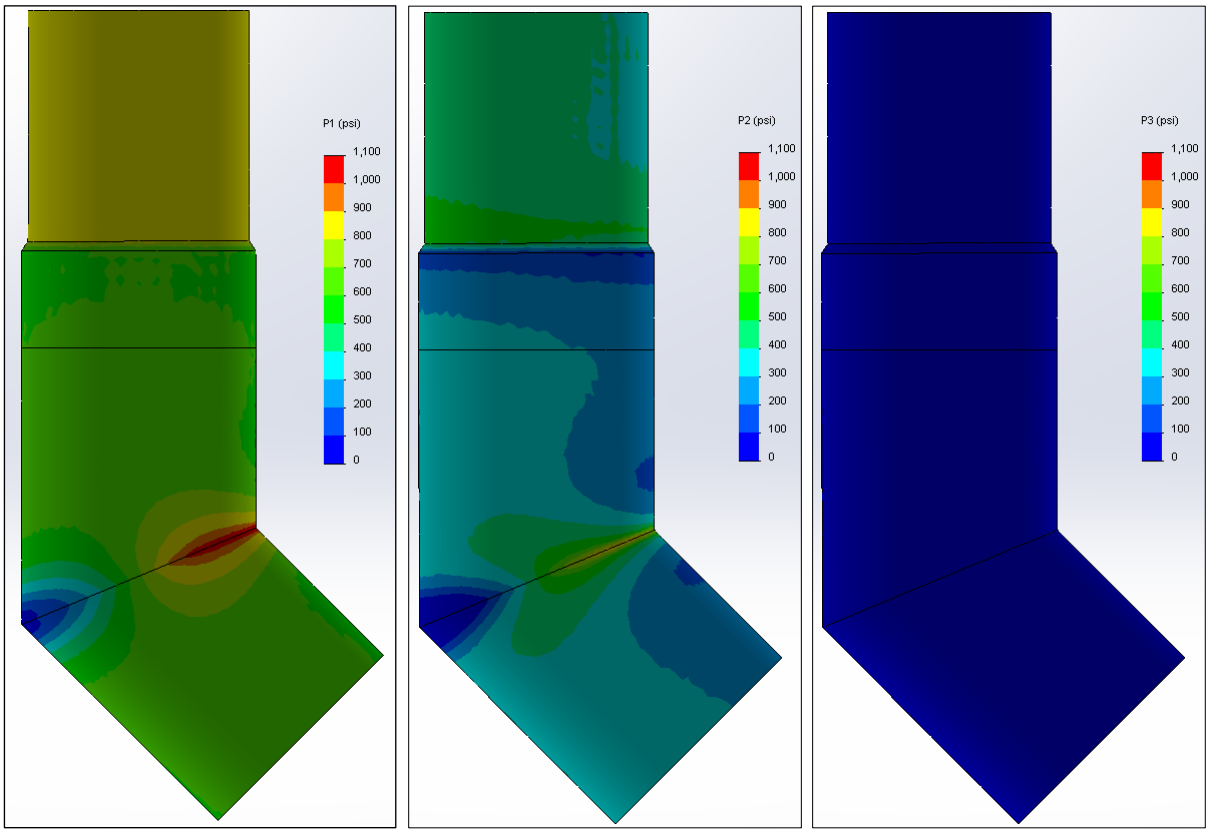

Figure 15. 3-segment bend, BRF=2.5, 1st, 2nd and 3rd principal stresses [psi] (left to right), external view, full model

The first and second principal stress plots indicate that higher stresses occur at the joint line, as expected. The third principal stresses (radial force due to pressure) are not significant in tension (i.e., < 100 psi).

Figure 16 shows a closer view of the first principal stress (hoop stress in straight pipe) at the joint line. From this external perspective the intrados is in tension and the extrados is in compression.

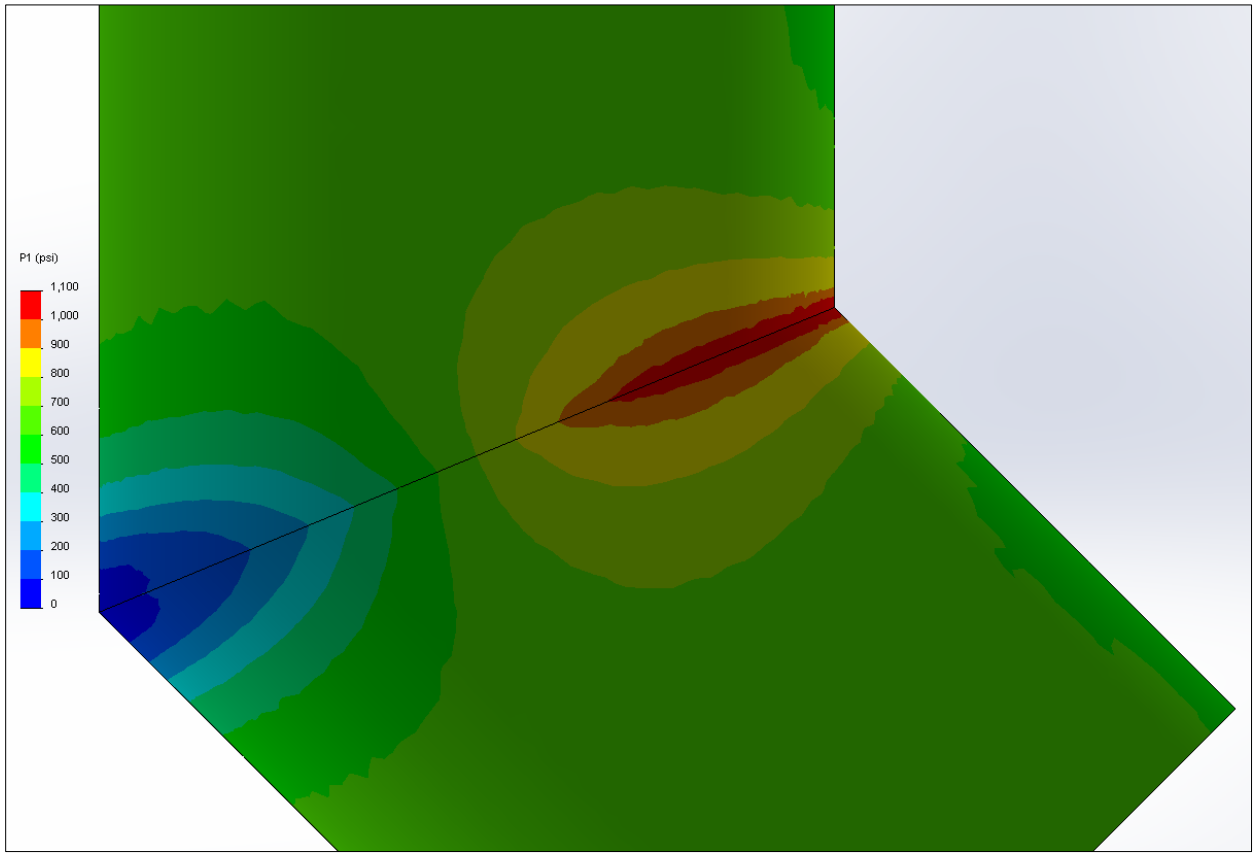

Figure 16. 3-segment bend, BRF=2.5, 1st principal (hoop) stress [psi], external view, joint

Figure 17 is similar to **Figure 15**, but showing stresses on the inside of the pipe and through its wall.

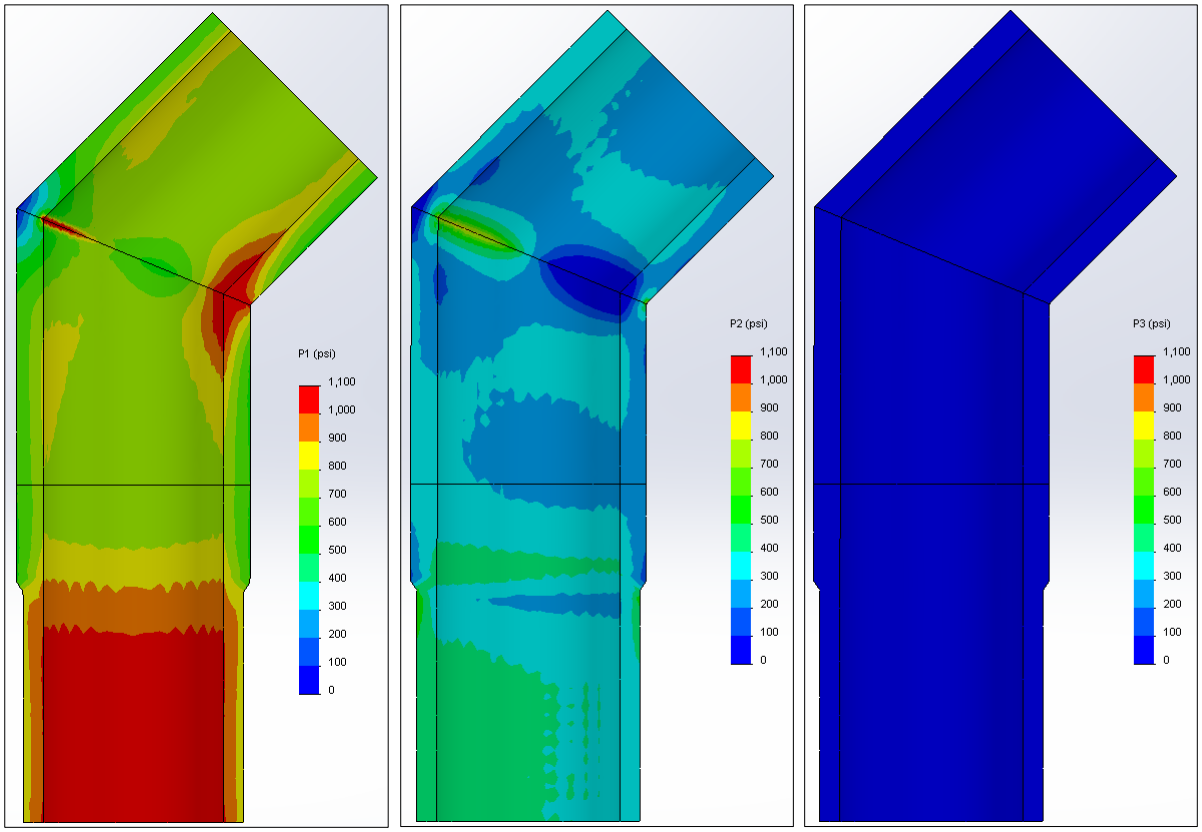

Figure 17. 3-segment bend, BRF=2.5, 1st, 2nd and 3rd principal stresses [psi] (left to right), internal view, full model

As can be seen from the first and second principal stress plots in **Figure 17**, the extrados corner of the joint experiences a sharp stress gradient from tension on the ID and compression on the OD. The intrados corner is in tension throughout the wall thickness. **Figure 18** shows this in more detail.

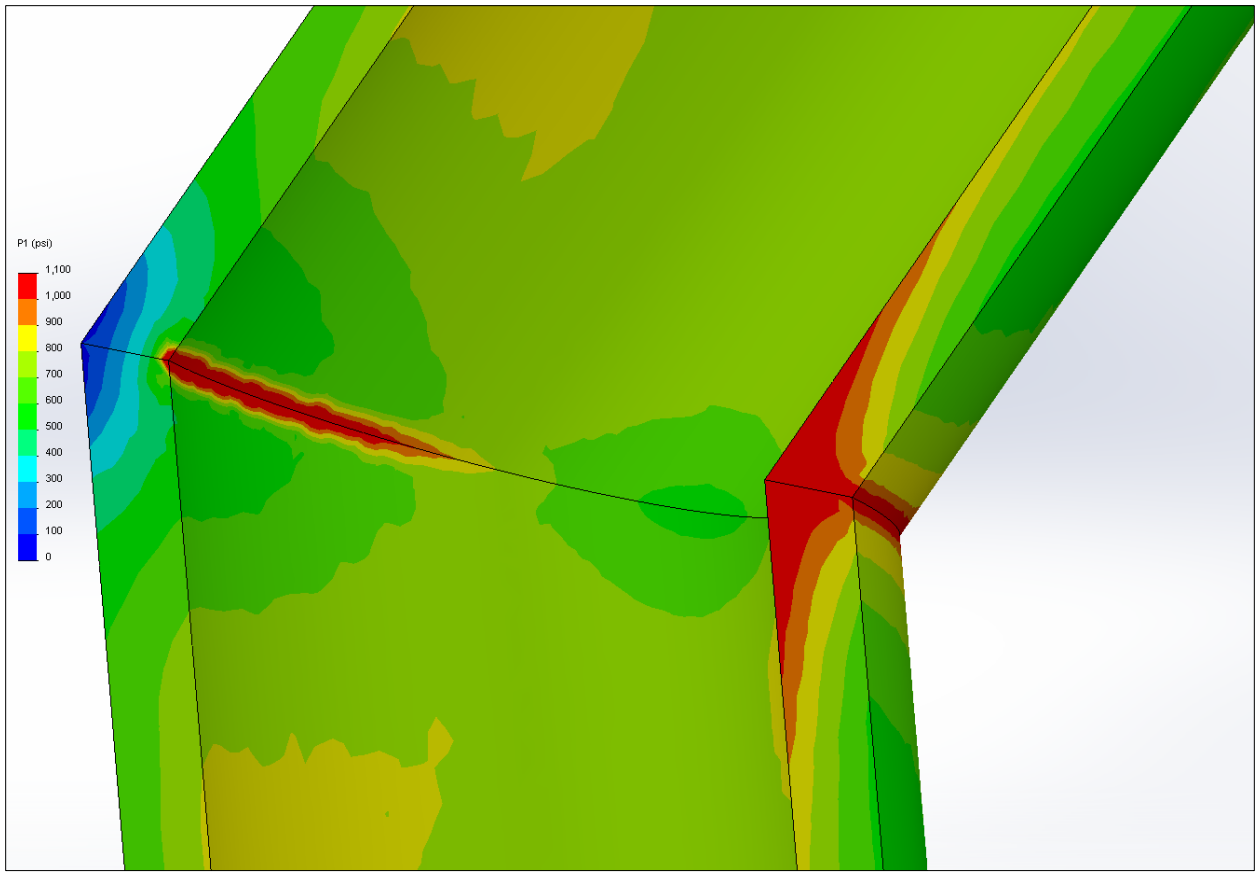

Figure 18. 3-segment bend, BRF=2.5, 1st principal (hoop) stress [psi], internal view, joint

The stress plots identify two locations where a failure could occur: the intrados corner and the ID at the extrados corner. This corresponds with field experience. Stress concentrations at the joint interface make fusion quality critical.

Figure 19 shows the von Mises stress from external and internal perspectives. As expected, the von Mises plot resembles the first principal stress plot in **Figure 17**.

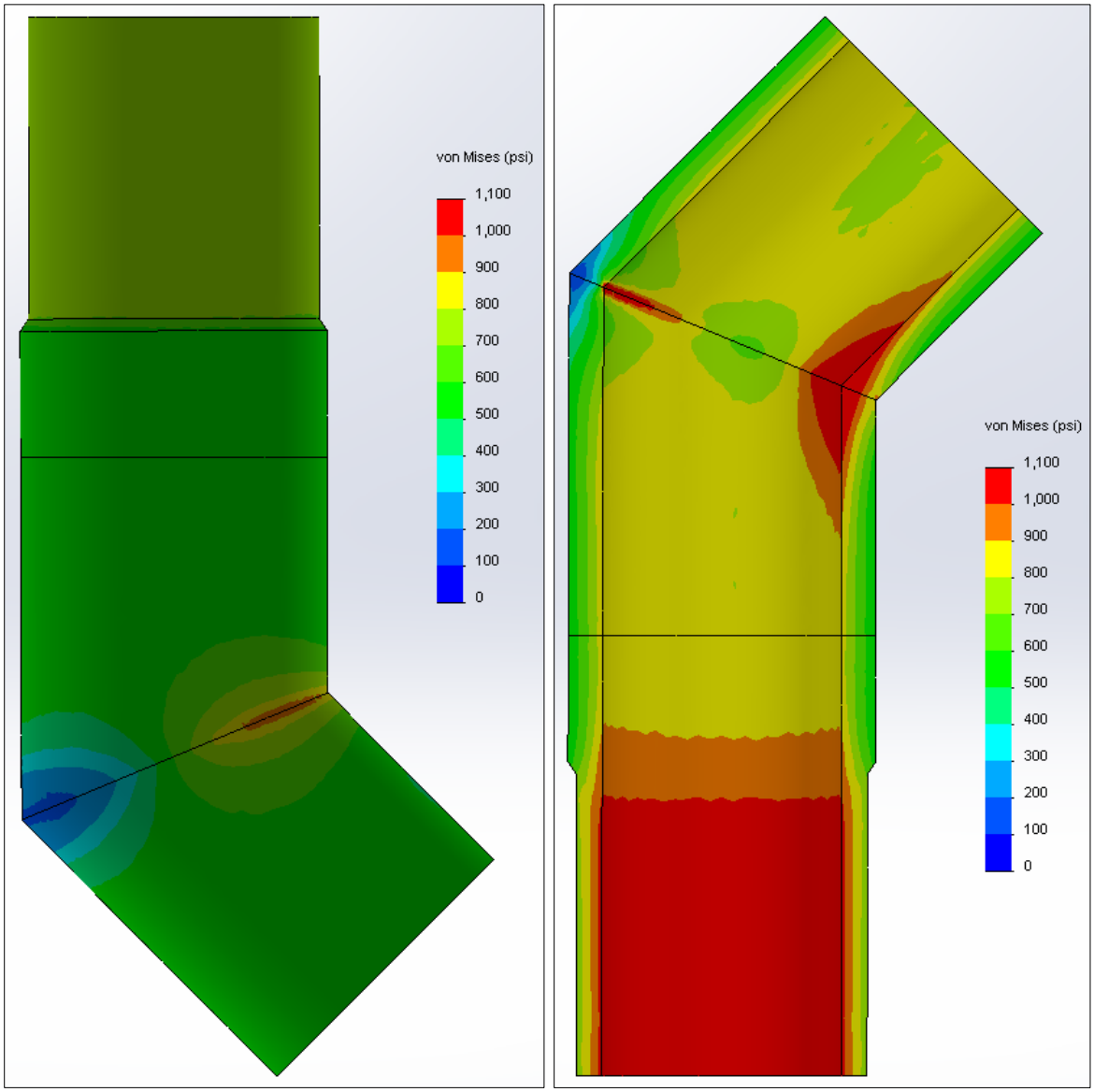

Figure 19. 3-segment bend, BRF=2.5, von Mises stress [psi], full model

Figure 20 and **Figure 21** show an example of a five-segment miter elbow with the same dimensions and boundary conditions as in the previous 3-segment example.

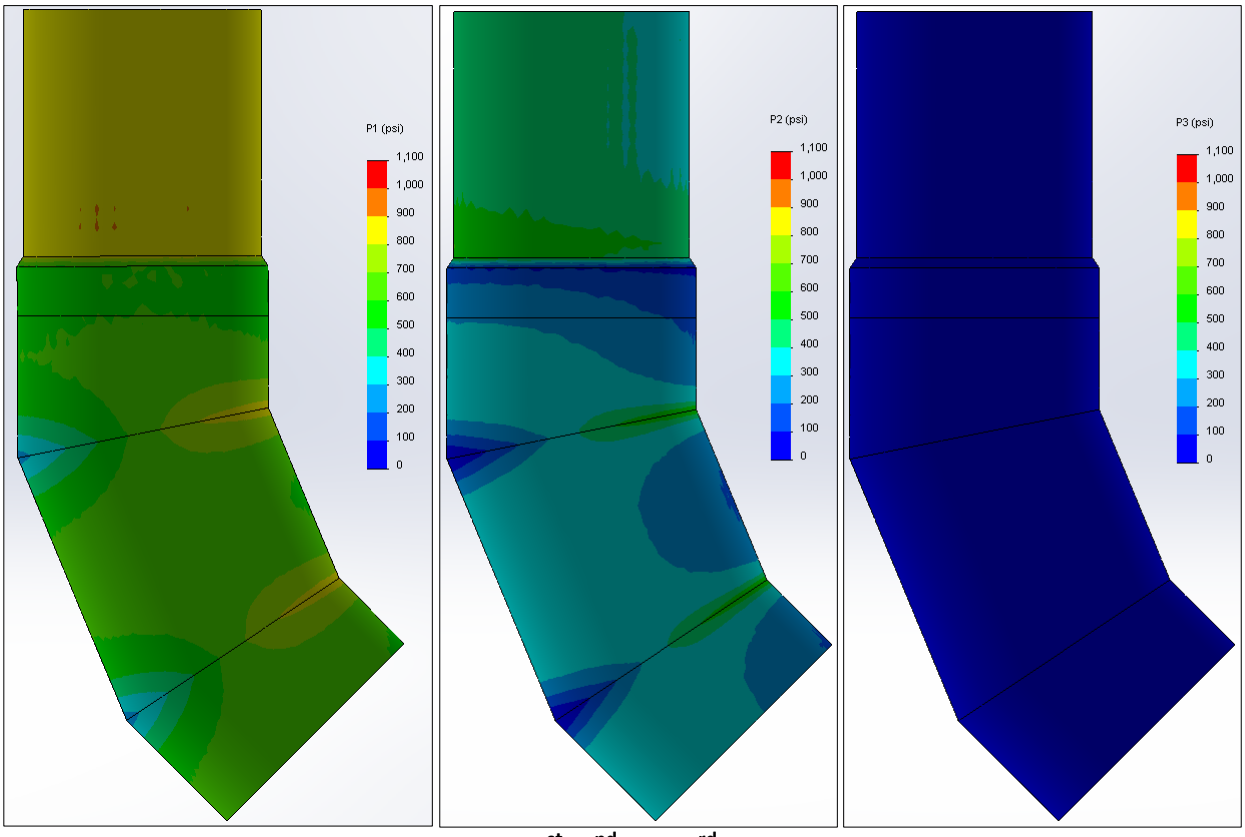

Figure 20. 5-segment bend, BRF=2.5, 1st, 2nd and 3rd principal stresses [psi] (left to right), external view, full model

Figure 20 already shows much lower stresses at the joint lines when compared to **Figure 16**. This illustrates the basic need for lower DRs at the miter segments as fewer segments are used.

Figure 21, again, shows the lower stresses of a five-segment elbow compared to a three-segment elbow (**Figure 17**).

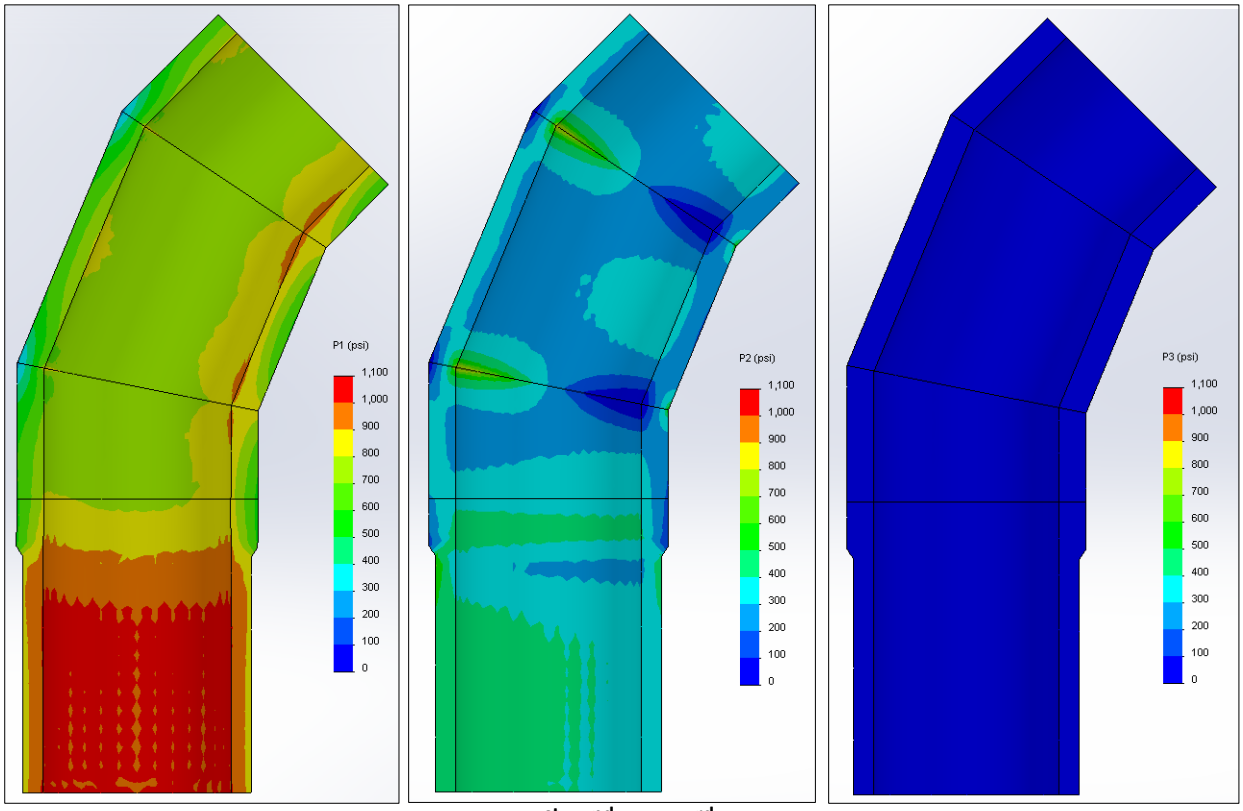

Figure 21. 5-segment bend, BRF=2.5, 1st, 2nd and 3rd principal stresses [psi] (left to right), internal view, full model

Effect of Bend Radius on Elbow Stress

The previous FEA study only considered a 2.5xOD bend radius (BRF=2.5) in its DoE matrix. This study expands from the previous study to include additional smaller bend radius factors (BRF): 1, 1.5, 2, and 2.5.

Figure 22 and **Figure 23** give a visual indication of the influence of bend radius on the stress field of externally and internally reinforced elbows, respectively.

Although the intrados stress does not change much (see **Figure 25**), the region of higher stress at the intrados corner begins to merge when the BRF is less than 1.5 (see top left images of **Figure 22** and **Figure 23**). There is good separation of the stress fields with bend radii larger than 1.5xOD. Of additional note is that the stress fields are very similar between externally and internally reinforced elbows with otherwise identical configurations.

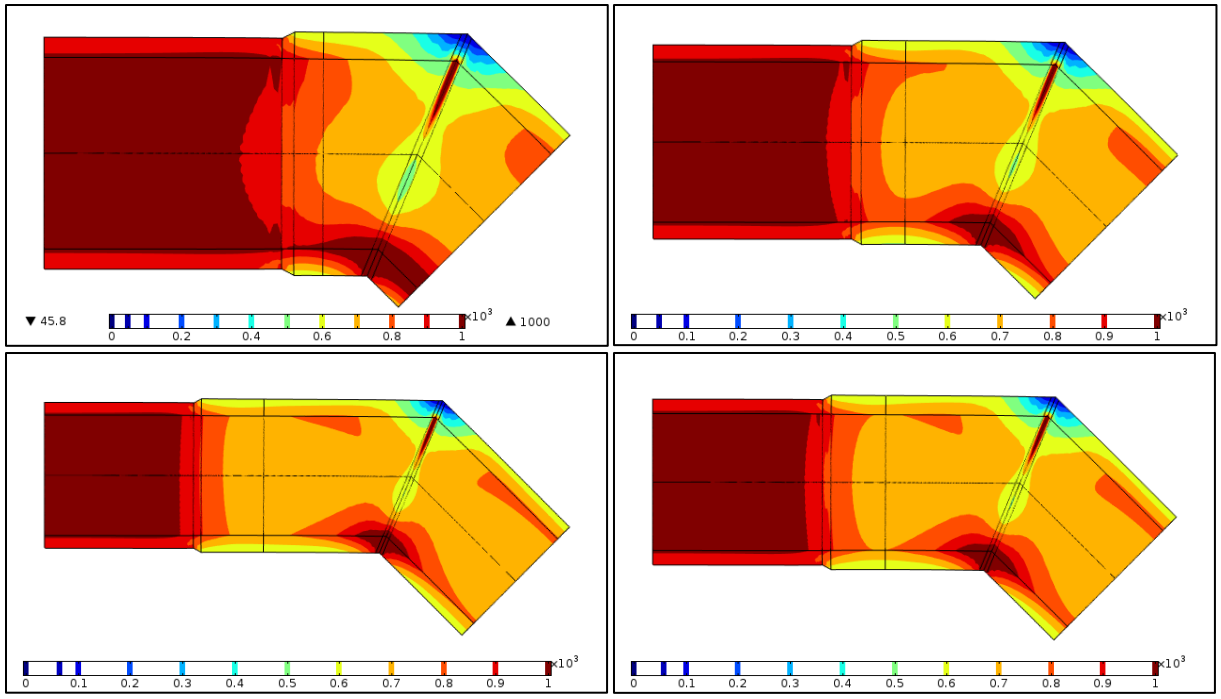

Figure 22. Effect of bend radius on externally reinforced elbow stress – 1.0xOD top left, 1.5xOD top right, 2.0xOD bottom right, 2.5xOD bottom left

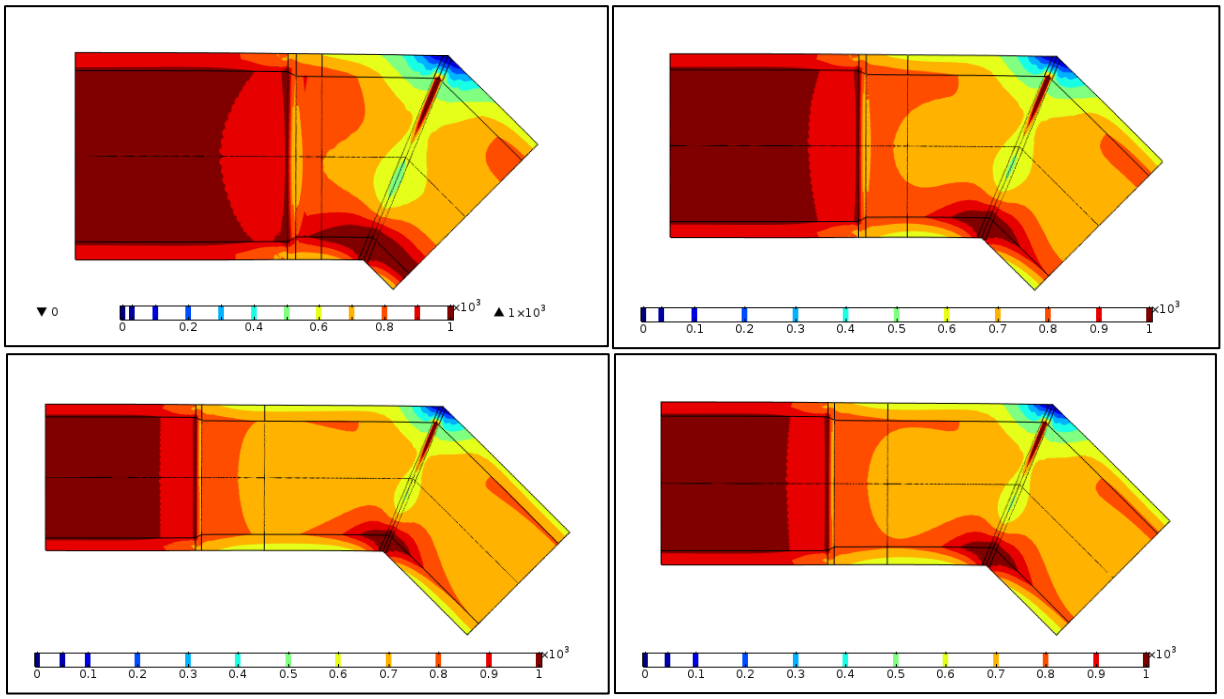

Figure 23. Effect of bend radius on internally reinforced elbow stress – 1.0xOD top left, 1.5xOD top right, 2.0xOD bottom right, 2.5xOD bottom left

The following path graphs help illustrate the stress merging caused by reducing the bend radius. **Figure 24** shows the intrados and extrados paths that were used for **Figure 25** through **Figure 27**.

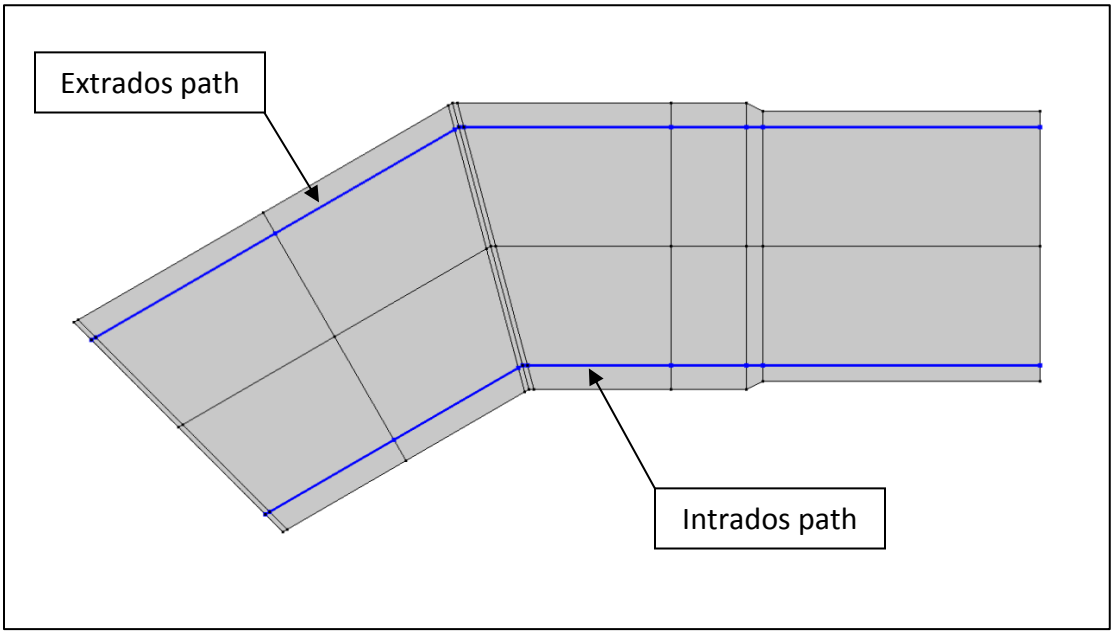

Figure 24. Probe paths (blue highlights) at intrados and extrados, as used in Figure 25 through Figure 27

Figure 25 shows the First Principal (hoop) stresses along the intrados and extrados of elbows with different bend radii. To show a worst-case, the stresses shown are from a 3-segment, DR 11, GSR 0.8 elbow at 200 psig, at 104°F.

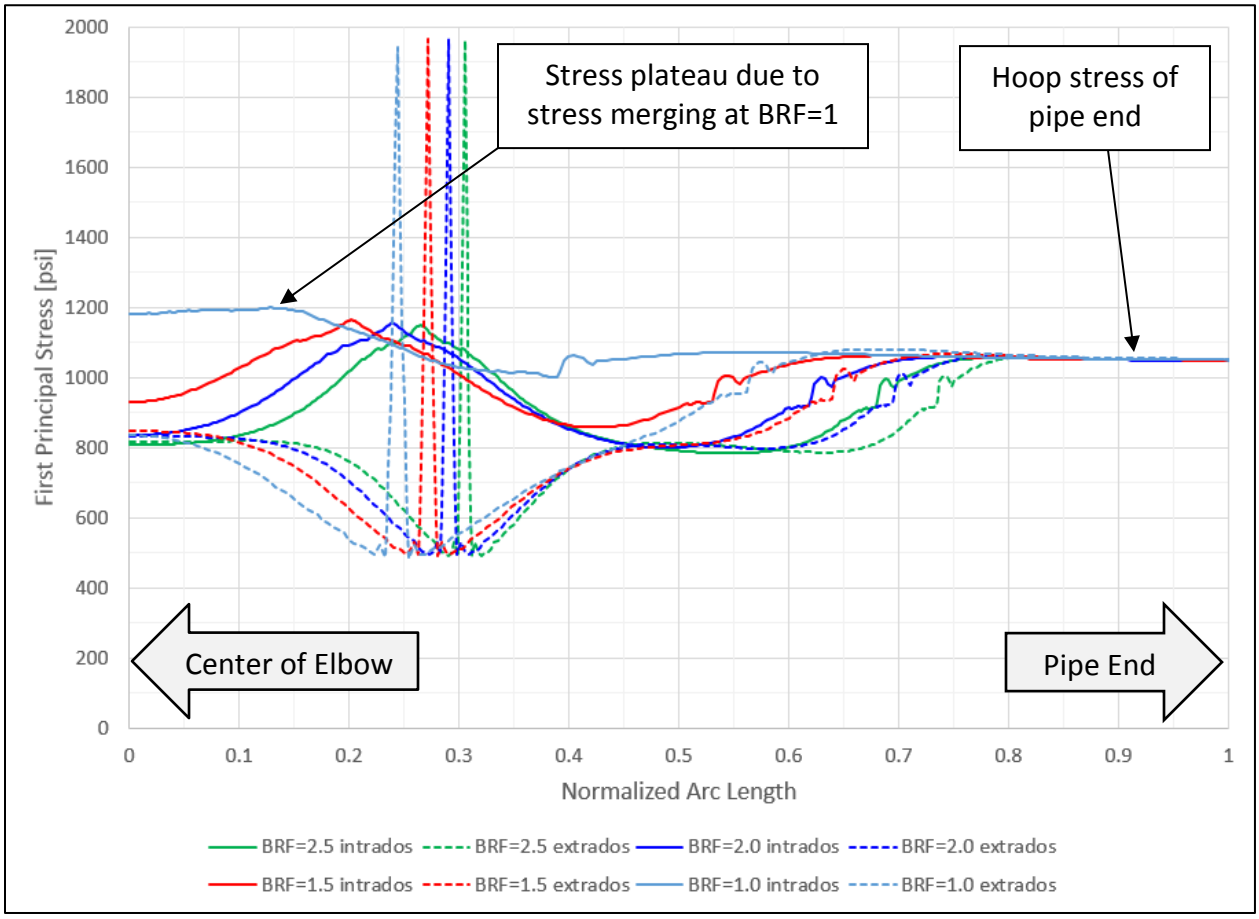

Figure 25. First Principal stress along intrados and extrados paths, at different bend radii, GSR=0.8

Note: The peak intrados stresses seen in **Figure 25**, **Figure 26**, and **Figure 27** are the highly localized stresses at the corner of miter segments. Since the design criterion used in this report is the average stress radially across the intrados wall thickness (see "intrados" line in **Figure 8**), an acceptable elbow configuration based on that criterion may still have peak stresses at its corners that exceed the nominal pipe hoop stress.

Figure 26 shows the same information as **Figure 25**, but for a configuration with GSR 0.6. The GSR 0.6 configuration has notably lower stresses, as expected.

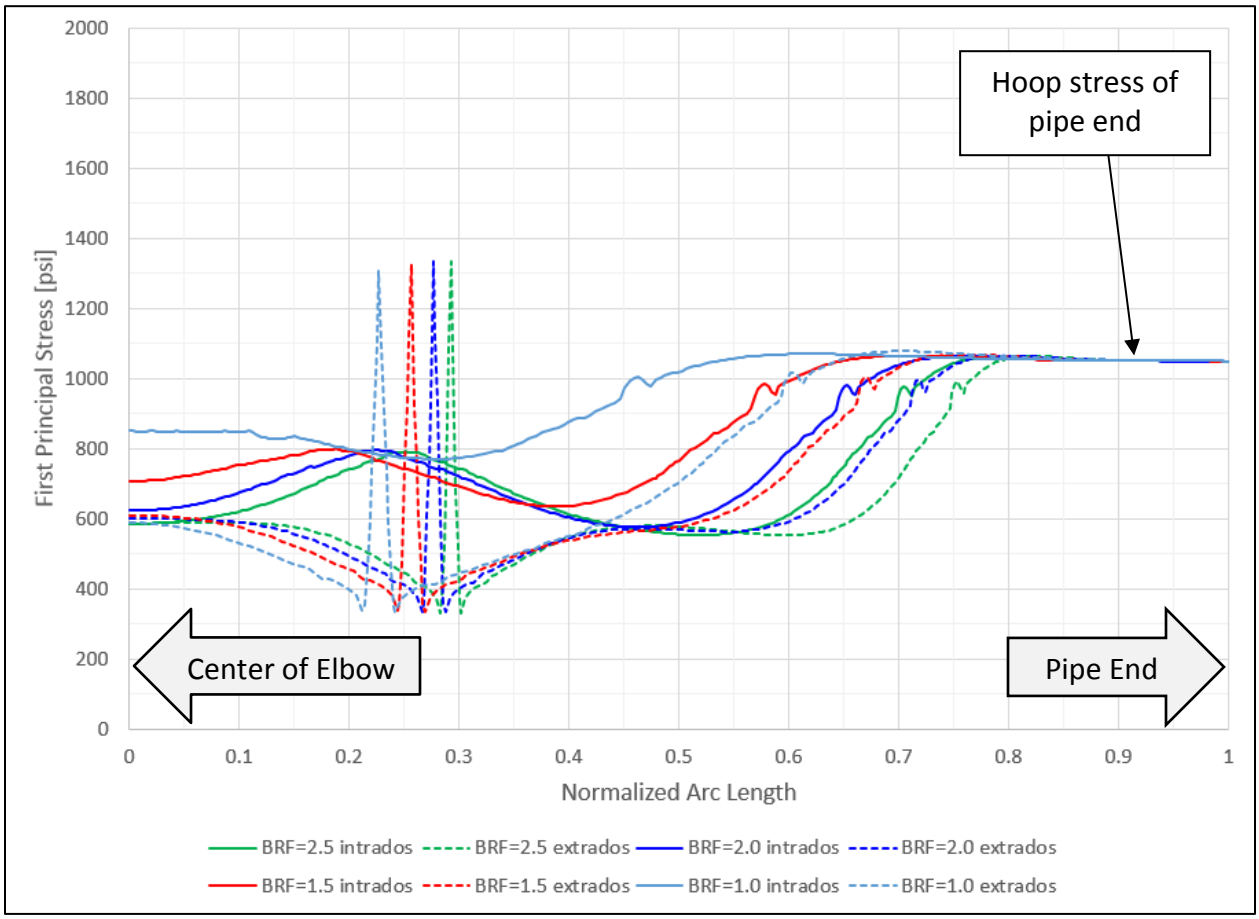

Figure 26. First Principal stress along intrados and extrados paths, at different bend radii, GSR=0.6

Figure 27 illustrates the effect of GSR by directly comparing the intrados path stresses of configurations with a GSR of 0.8 with configurations with a GSR of 0.6.

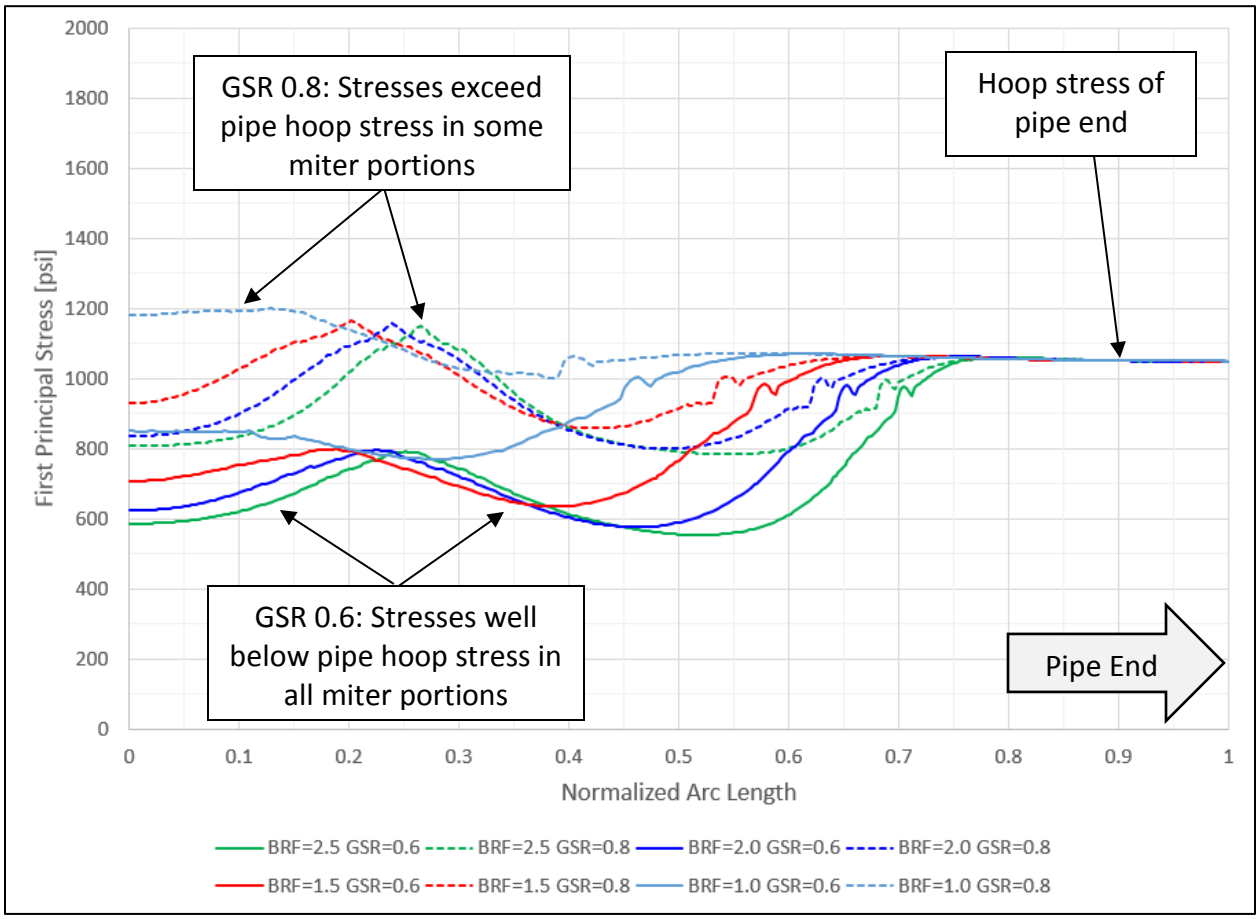

Figure 27. First Principal stress along intrados path, at different bend radii, GSR=0.6 vs. GSR=0.8

Fusion Beads

An attempt was made to analyze the miter bends with beads, however, because of their complexity; they had to be modeled individually, per configuration. This precluded their use within the scope of this project and therefore only a single model with fusion beads was analyzed for reference.

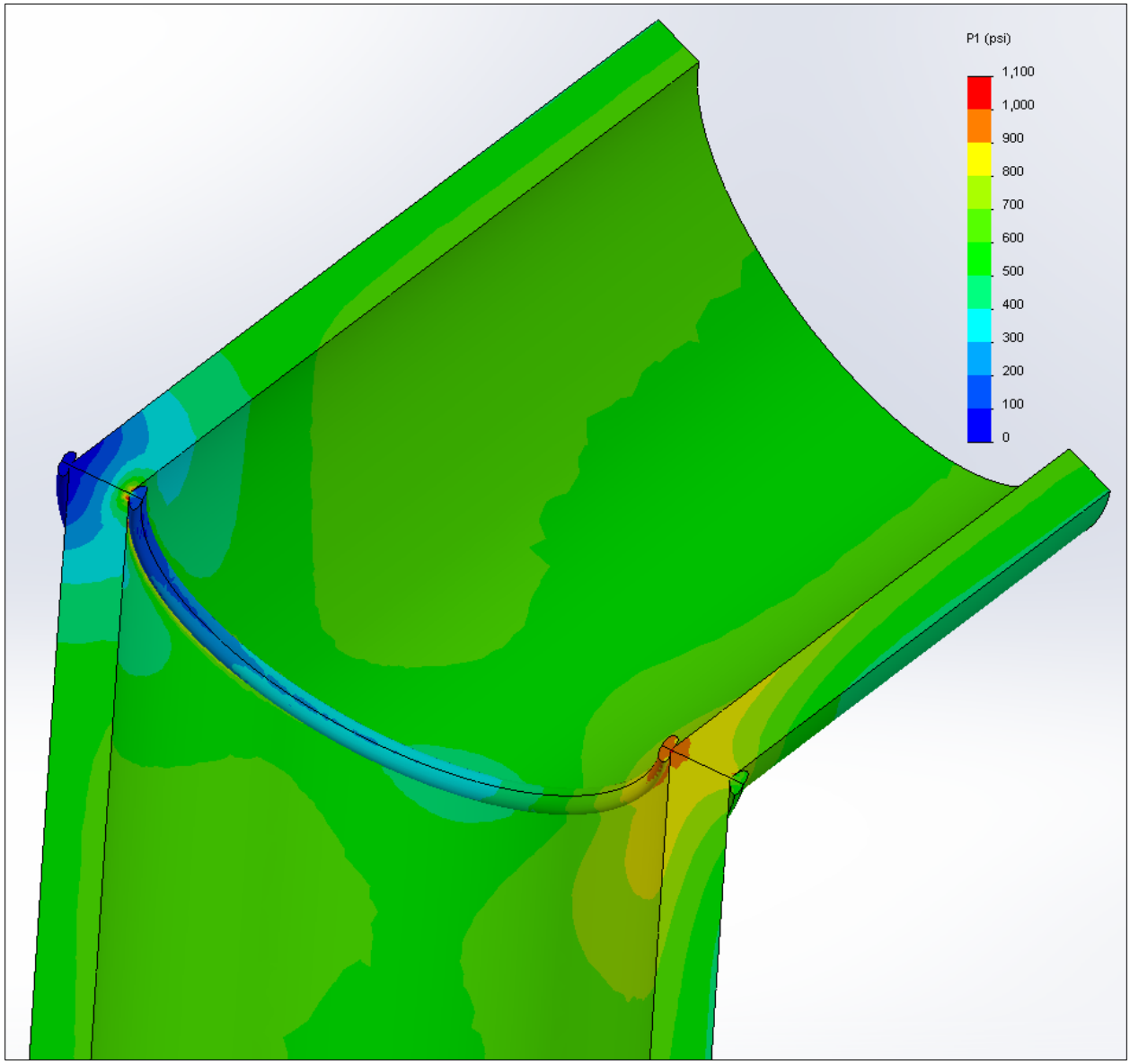

Figure 28. 3-segment bend, 1st principal (hoop) stress [psi], internal view, joint with bead

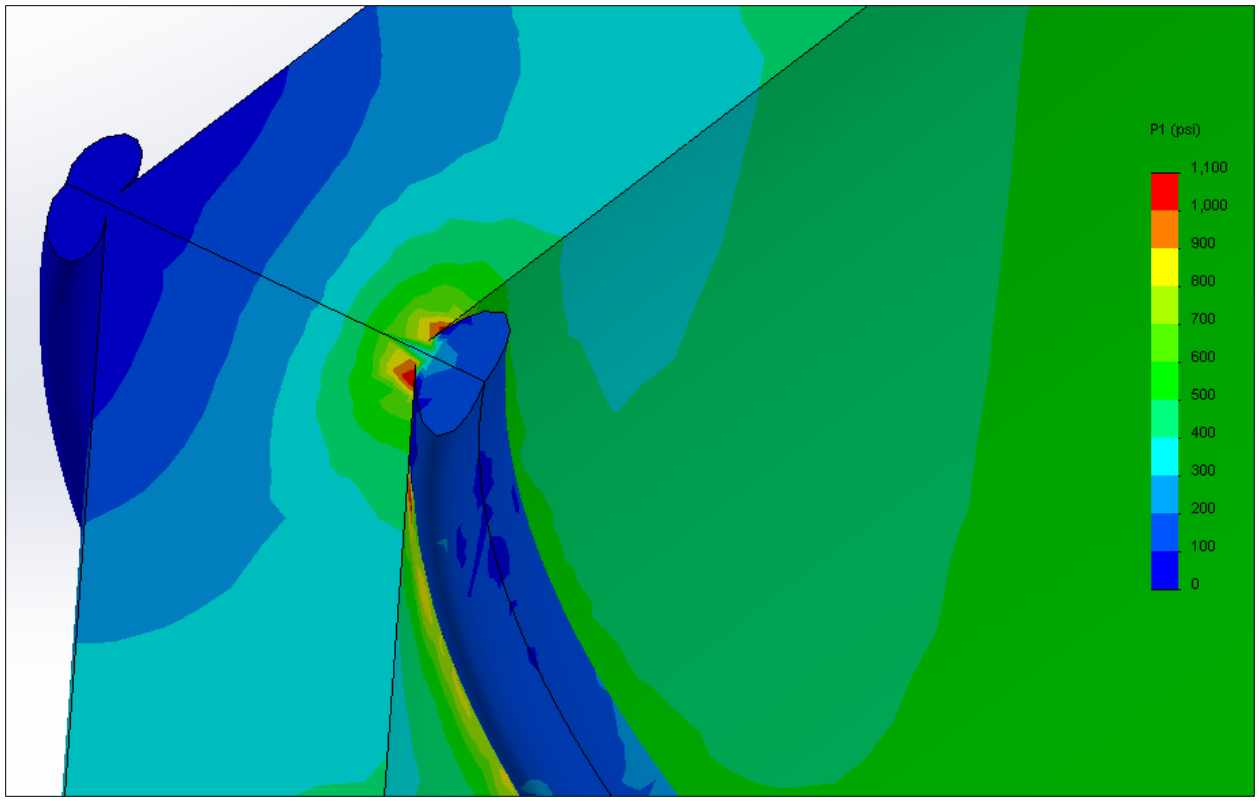

Figure 29. 3-segment bend, extrados hoop stress [psi], internal view close-up, joint with bead

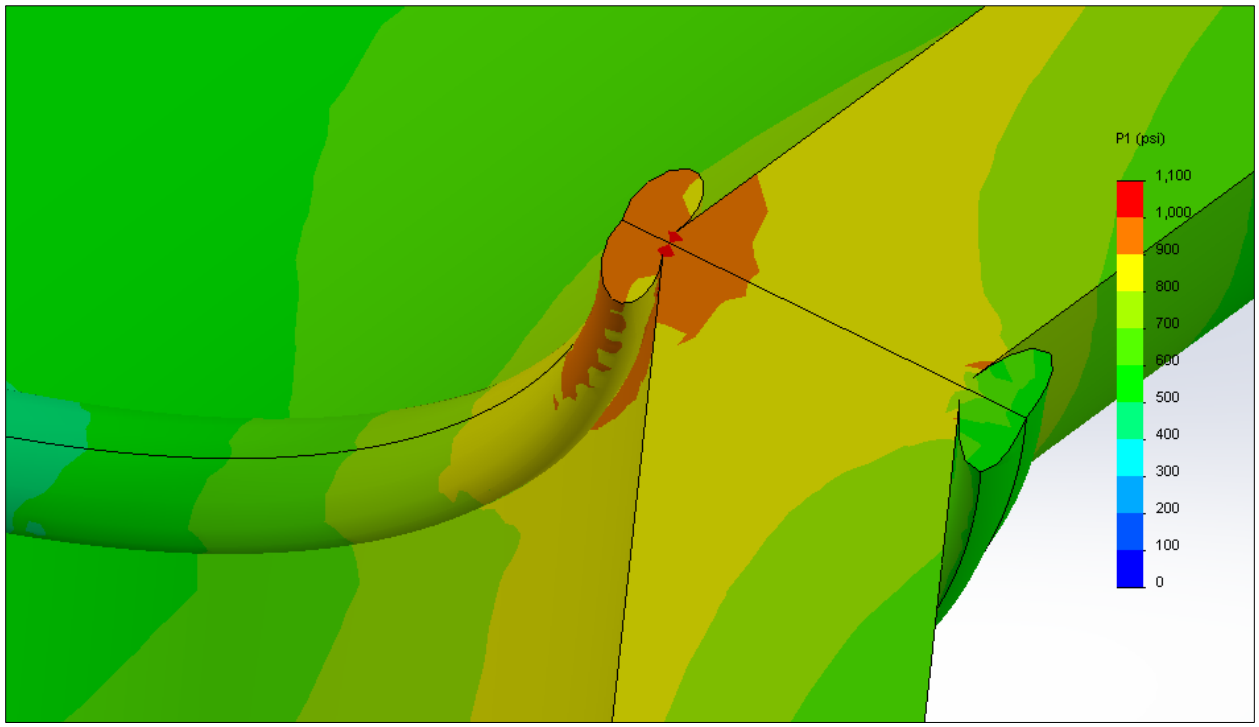

Figure 30. 3-segment bend, intrados hoop stress [psi], internal view close-up, joint with bead

As can be seen in **Figure 29** and **Figure 30**, the fusion beads reduce the hoop stress at the very center of the joint, but cause a stress concentration where each bead meets the inner pipe

wall. **Figure 31** shows a comparison of hoop stresses on a model with and without beads. **Figure 32** and **Figure 33** show the extrados and intrados in detail, respectively.

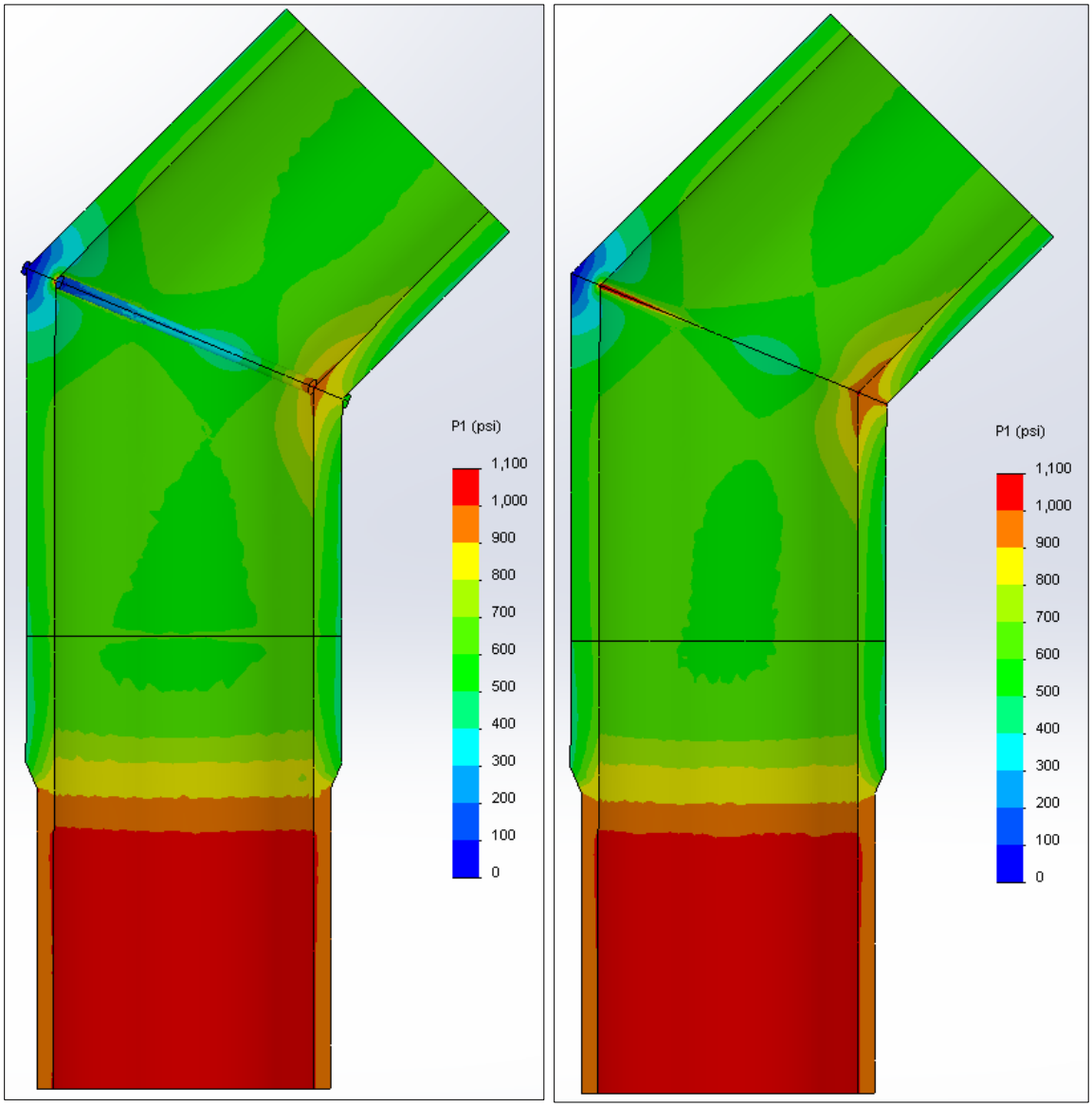

Figure 31. Comparison of hoop stress [psi] on model with and without beads, full model

Figure 31 illustrates how the bead only affects stresses in its close vicinity. **Figure 33** shows how ignoring the beads results in a higher average hoop stress at the intrados corner. The inner bead, however, may cause higher stresses at the edge of its contact with the pipe's inner wall. This will require further investigation.

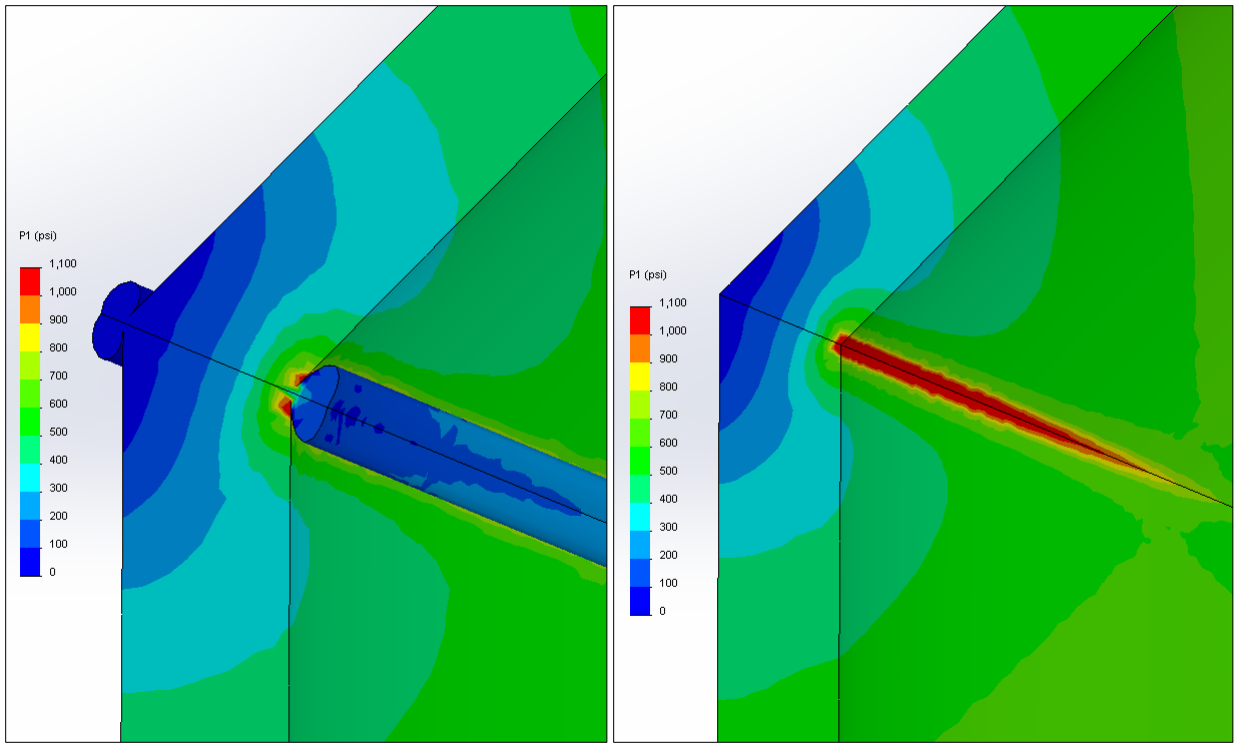

Figure 32. Comparison of hoop stress [psi] on model with and without beads, extrados

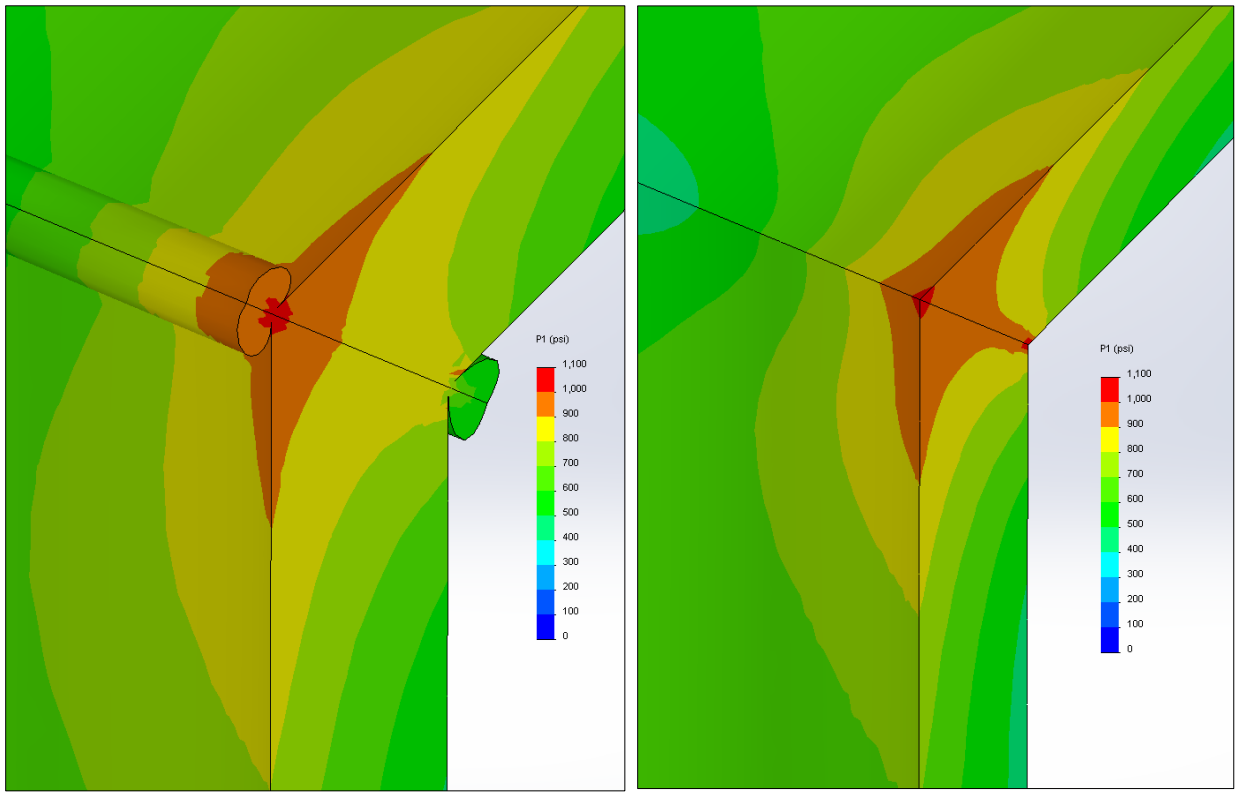

Figure 33. Comparison of hoop stress [psi] on model with and without beads, intrados

Mesh Quality

The sensitivity of the FEA result to mesh density was checked. The results are presented in **Figure 34** below. The ratio between the results for the average intrados first principal stress that is used as the basis for this analysis was 0.99985 (high resolution mesh result / low resolution mesh result). The mesh resolution used in the DoE overestimates the high quality mesh result by less than one tenth of a percent (15 thousandths of a percent).

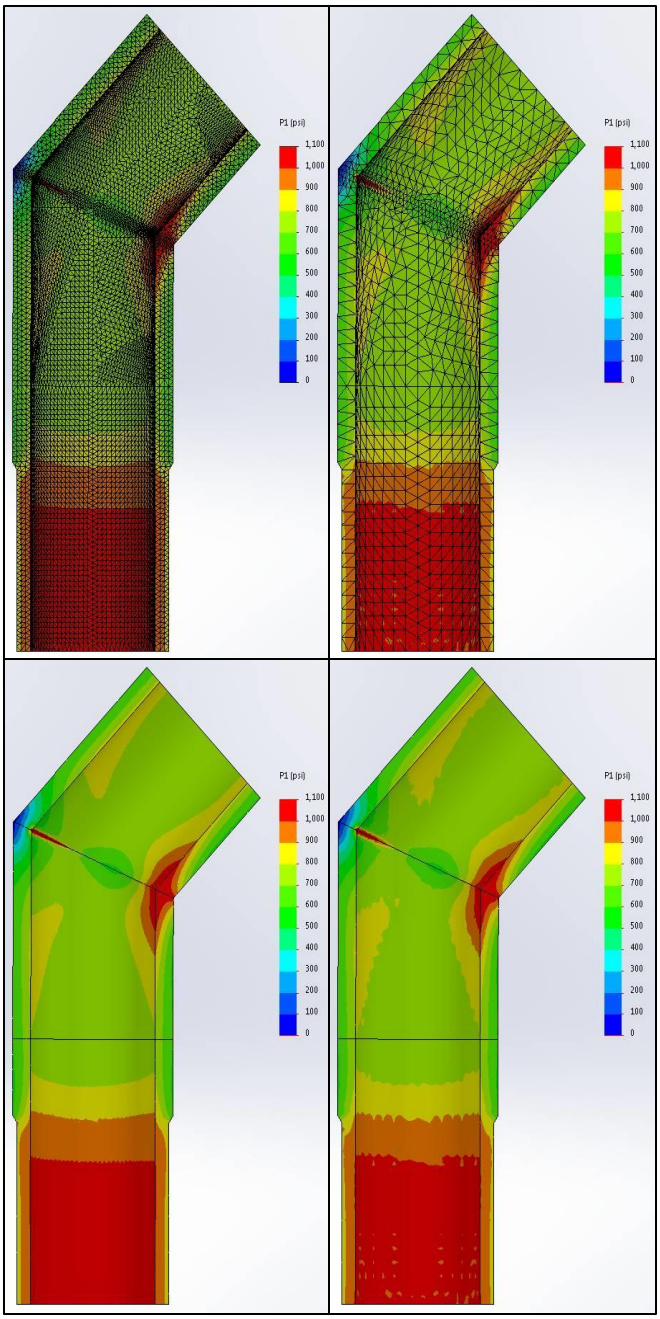

Figure 34. Mesh quality check

Reference Stress for Calculations

The intrados average first principal stress is always the largest stress in the mitered elbow as can be seen in **Figure 26**. This stress is used in all subsequent calculations and models requiring a stress input. In a straight pipe segment the first principal stress corresponds to the hoop stress of the pipe, which is the reference stress used in all pipe design calculations. For consistency this is the reference stress we have used in this report. The relative values of the first, second and third principal stresses can be seen in **Figure 15** through **Figure 30**. It is also clear in reviewing these plots that there is little difference between the stress patterns of the first principle stress and the von Mises stress in all of the elbow configurations.

In a DR 11 pipe the third principal stress (radial) is the internal pressure in the pipe, the first principal stress (hoop) is 5 times the internal pressure and the second principal stress (axial) is 2.5 times the internal pressure. The von Mises stress is 1.04403 times the first principal stress, i.e., less than 5% higher.

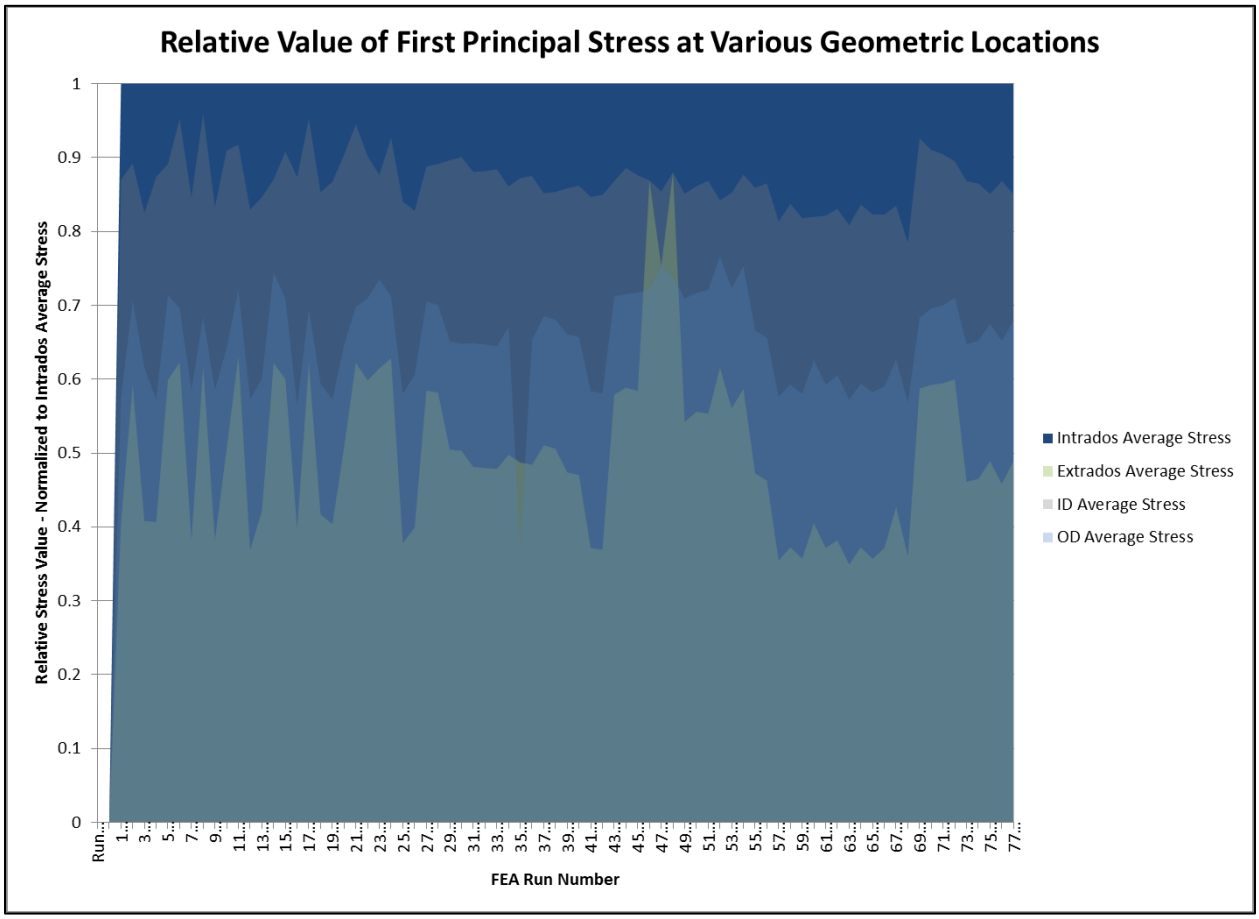

Figure 35. Relative Values of First Principal Stress at Various Geometric Locations

Comparison of FEA results to ASME Design Equations for Mitered Elbows

ASME B31.3-2012 Section 304.2.3 Miter Bends provides equation (4a) referenced as **Equation 1** for calculating the maximum allowable pressure in a mitered elbow with miter cut angle θ less than or equal to 22.5°:

$$P_m = \frac{S\,E\,W\,(T-c)}{r_2}\left(\frac{T-c}{(T-c)+0.643\tan\theta\sqrt{r_2(T-c)}}\right) \qquad \textbf{Equation 1}$$

P_m	maximum allowable internal pressure
c	sum of the mechanical allowances
D	outside diameter of pipe
r_2	mean radius of pipe using nominal wall T
E	quality factor *P*p internal design gage pressure
S	stress value for material
T	pipe wall thickness (measured or minimum in accordance with the purchase specification)
t_m	minimum required thickness, including mechanical, corrosion, and erosion allowances
W	weld joint strength reduction
θ	Miter cut angle

Setting E and W = 1 and defining (T-c) as "t" we get a simplified equation:

$$P_m = \frac{S\,t}{r_2}\left(\frac{t}{t+0.643\tan\theta\sqrt{r_2 t}}\right) \qquad \textbf{Equation 2}$$

t	pressure design thickness

Equation 2 can be manipulated to give:

$$\frac{P_m r_2}{S} = \mathrm{t}\left(\frac{t}{t+0.643\tan\theta\sqrt{r_2 t}}\right) = \left(\frac{t}{1+0.643\tan\theta\sqrt{\frac{r_2}{t}}}\right) \qquad \textbf{Equation 3}$$

Recognizing that the LHS of **Equation 3** is the nominal pipe wall thickness t_0 we can rearrange the equation to give:

$$\mathrm{t} = t_0\left(1 + 0.643\sqrt{\frac{r_2}{t}}\tan\theta\right) \qquad \textbf{Equation 4}$$

Equation 4 is useful for calculating the required wall thickness for a mitered elbow. This equation is derived from the work of Green and Emmerson [1] who solved the elasticity problem of an unrestrained discontinuous bend. The solution developed by Green and Emmerson has been extensively validated for steel mitered elbows. Wood [2] used this equation to validate the finite element solution he developed for steel mitered elbows. We will

now use this equation to validate that the non-linear finite element study carried out by GTI is consistent with the ASME design approach. To accomplish this validation we parameterize **Equation 4** as follows:

$$\mathbf{t} = \boldsymbol{t_0}(\mathbf{1} + \boldsymbol{a}\sqrt{\frac{r_2}{t}}\tan\boldsymbol{\theta}) \qquad \textbf{Equation 5}$$

Next we fit a model of form described in **Equation 5** to the full set of FEA results, which includes the original (BRF=2.5) data set and the new data with the expanded range of BRF factors (1.5 to 2.5), and extract the value of parameter "a" that provides the best fit.

$$\frac{P_m r_2}{t} = \mathbf{S}\left(\mathbf{1} + \boldsymbol{a}\tan\boldsymbol{\theta}\sqrt{\frac{r_2}{t}}\right) \qquad \textbf{Equation 6}$$

Figure 36 and
Figure 37 below show the results of the model fit and the 95% confidence surfaces respectively. The adjusted R^2 of the model is 0.9605 and:

a = 0.3073 (0.2924, 0.3223)

This fitted value of the parameter "a" is valid for all temperatures in the range 32°F – 104°F, all miter cut angles less than or equal to 22.5°, and bend radius factors of 1.5 to 2.5. This is an extremely encouraging result as it shows that the non-linear temperature dependent stress-strain curves used in the analysis correctly capture the elastic behavior of the elbows across the range of loading conditions, elbow geometry, and temperatures used in the study.

A very simple design equation for the required thicker wall of the elbow results:

$$\mathbf{t} = \boldsymbol{t_0}(\mathbf{1} + \mathbf{0.3073}\sqrt{\frac{r_2}{t}}\tan\boldsymbol{\theta}) \qquad \textbf{Equation 7}$$

Equation 7 for HDPE mitered elbows reflects the fact that plastic materials are much more compliant than steel and develop lower stress risers as a result (a=0.3073 as opposed to a=0.643 for steel).

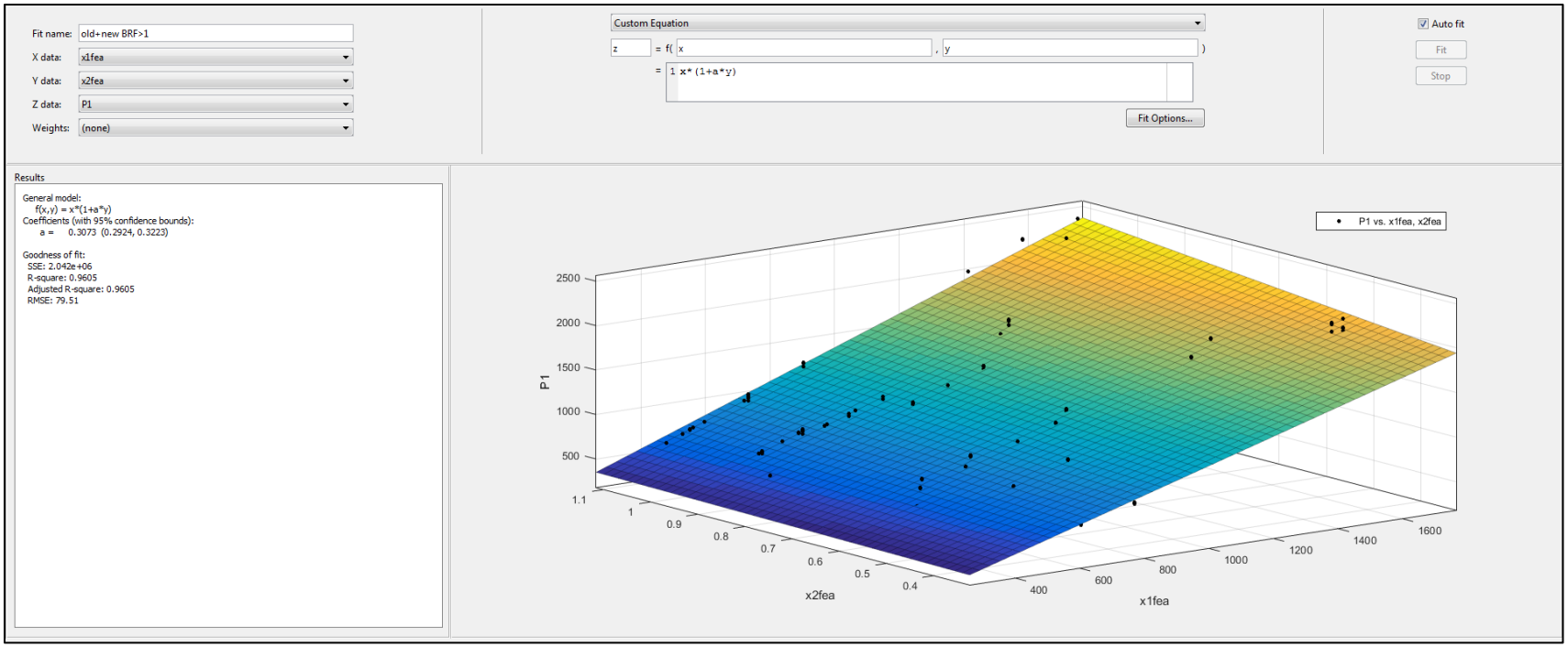

Figure 36. Fit of FEA results to Equation 5 to determine parameter "a", for BRF>=1.5

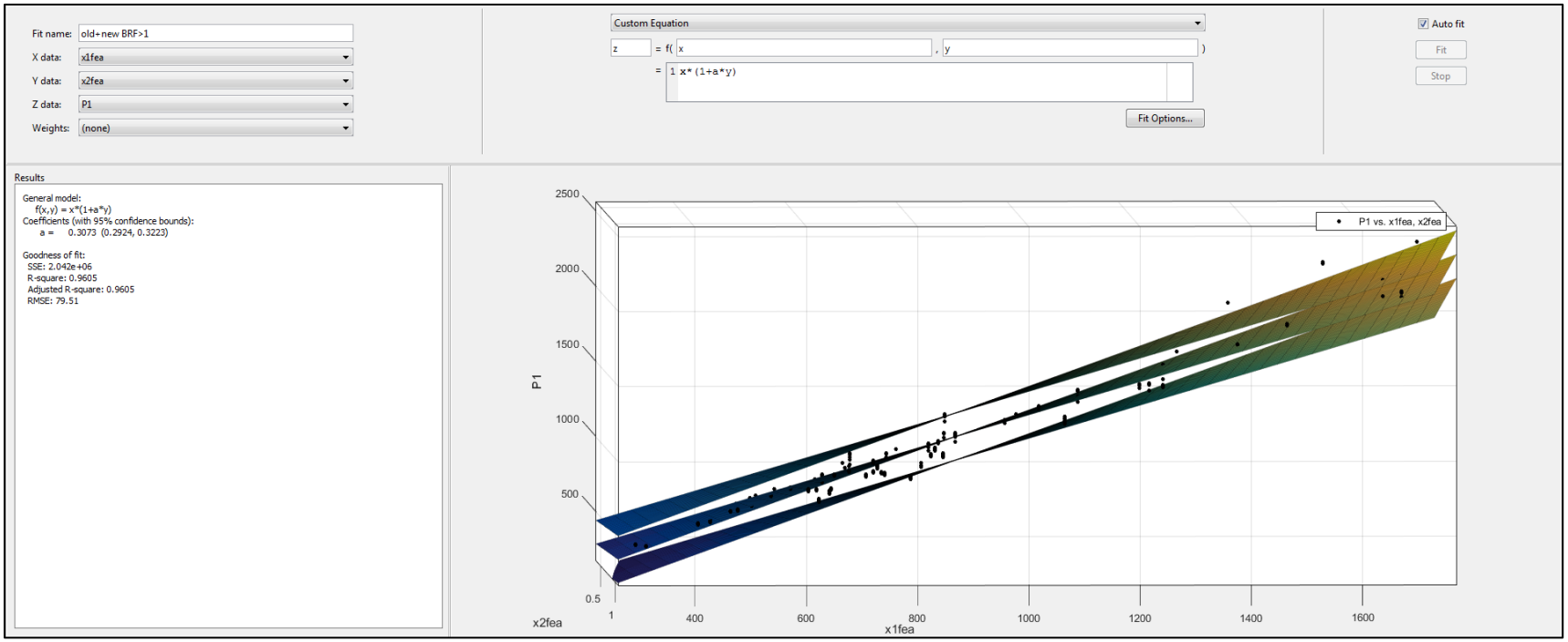

Figure 37. 95% Prediction surfaces for FEA model fit, for BRF>=1.5

Recognizing that:

$$\sqrt{\frac{r_2}{t}} = \sqrt{\frac{D-t}{2t}} = \frac{1}{\sqrt{2}}\sqrt{\frac{D}{t}-1} = \frac{1}{\sqrt{2}}\sqrt{DR-1}$$

Substituting in **Equation 7** gives us:

$$\mathbf{t} = \boldsymbol{t_0}\left(\mathbf{1} + \frac{\mathbf{0.3073}}{\sqrt{\mathbf{2}}}\sqrt{\boldsymbol{DR}-\mathbf{1}}\,\mathbf{\tan}\,\boldsymbol{\theta}\right) \qquad \textbf{Equation 8}$$

Equation 8 can be used directly to calculate the necessary increase in wall thickness as a function of miter cut angle and pipe dimension ratio, DR=D/t. The results of this calculation for a range of miter cut angles 2.813° - 22.5° and DRs ranging from 7 – 32.5 are presented in **Table 3**. The Geometric Strength Ratio (GSR) is the inverse of the wall thickness multiplier and can be used to calculate the appropriate DR for the fabricated elbow.

$$\mathbf{GSR} = \frac{\mathbf{1}}{\mathbf{1}+\mathbf{0.3073}\sqrt{\frac{r_2}{t}}\mathbf{\tan}\,\boldsymbol{\theta}} \qquad \textbf{Equation 9}$$

The results in **Table 3** show that, the current industry practice of using a DR of one standard dimension less than the pipe for the fabricated elbow, which results in an approximately 25% increase in wall thickness, is a very reasonable approach and is nominally conservative up to a miter cut of 22.5° and for DRs less than or equal to 21.

Table 3. Calculated GSR values (BRF>=1.5), a=0.3073

Pipe DR	Θ	Wall Thickness Multiplier	Geometric Strength Ratio (GSR)
7	5.625	1.0524	0.95
9	5.625	1.0605	0.94
11	5.625	1.0677	0.94
13	5.625	1.0741	0.93
15	5.625	1.0801	0.93
17	5.625	1.0856	0.92
19	5.625	1.0908	0.92
21	5.625	1.0957	0.91
26	5.625	1.1070	0.90
32.5	5.625	1.1201	0.89
7	11.250	1.1059	0.90
9	11.250	1.1223	0.89
11	11.250	1.1367	0.88
13	11.250	1.1497	0.87
15	11.250	1.1617	0.86
17	11.250	1.1729	0.85
19	11.250	1.1834	0.85
21	11.250	1.1933	0.84
26	11.250	1.2161	0.82
32.5	11.250	1.2426	0.80
7	15.000	1.1426	0.88
9	15.000	1.1647	0.86
11	15.000	1.1841	0.84
13	15.000	1.2017	0.83
15	15.000	1.2179	0.82
17	15.000	1.2329	0.81
19	15.000	1.2470	0.80
21	15.000	1.2604	0.79
26	15.000	1.2911	0.77
32.5	15.000	1.3268	0.75
7	22.500	1.2205	0.82
9	22.500	1.2546	0.80
11	22.500	1.2846	0.78
13	22.500	1.3118	0.76
15	22.500	1.3368	0.75
17	22.500	1.3600	0.74
19	22.500	1.3819	0.72
21	22.500	1.4025	0.71
26	22.500	1.4500	0.69
32.5	22.500	1.5052	0.66

To help use the data in **Table 3**, **Figure 38** shows the data in terms of GSR versus Pipe DR.

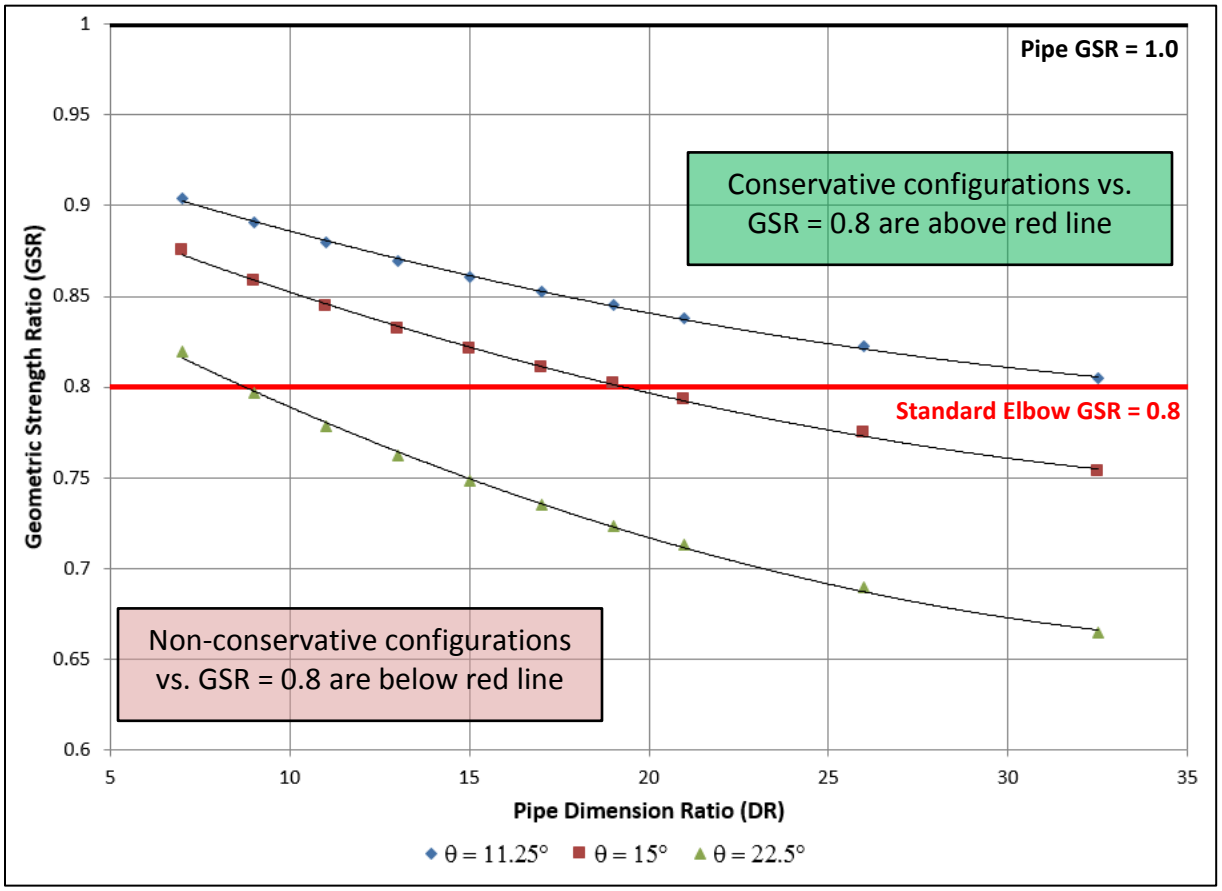

Figure 38. GSR versus Pipe DR for different miter angles with BRF>=1.5, from Table 3.

Note

The value of "a" calculated in GTI PROJECT NUMBER 02222-121534 was 0.2856. The value calculated in this analysis using the COMSOL Multiphysics finite element solvers is 5.7% greater (0.3019) for the same geometry configurations and material model. This reflects the greater stiffness of the tighter BRFs of 2.0 and 1.5 that were included in the current analysis. The tighter bend radii increase the stiffness of the elbows, thus increasing the parameter "a". The value for "a" calculated here (0.3019) lies between the mean and upper confidence level of the original analysis i.e. there is no statistical difference between the two results.

Including BRF=1 further increases this value to 0.3213, which is 12.5% greater than the original 0.2856.

To better illustrate how the “a” parameter is influenced by BRF, **Figure 39** shows the value of the “a” parameter as a function of BRF. The fitted curve is shown for illustrative purposes only. As can be seen, there is a marked increase in parameter “a” at BRF=1 versus BRF=1.5. Furthermore, BRF 1.5, 2.0 and 2.5 have similar “a” values, indicating that a single “a” value can be used for BRF>=1.5, while a different “a” value should be used for BRF=1.

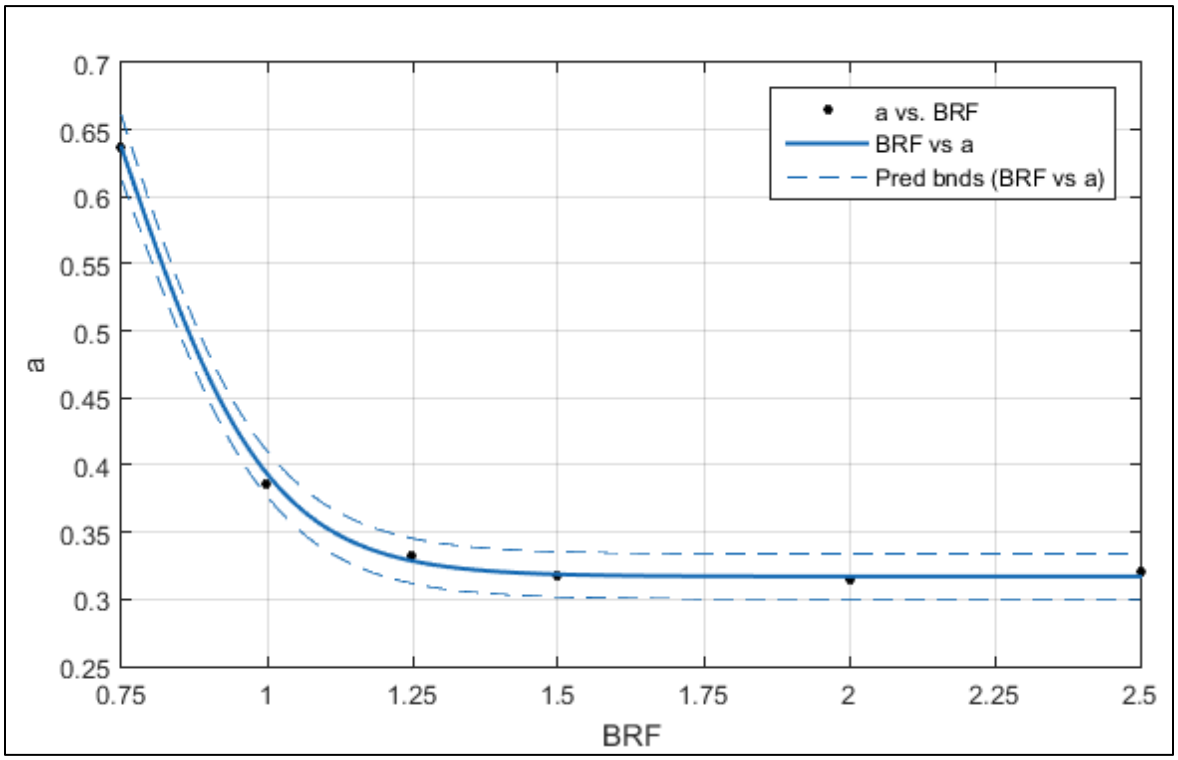

Figure 39. Plot of “a” versus BRF, with illustrative curve fit and 99% prediction bounds

Figure 40 and **Figure 41** show the Equation 5 fits to the FEA results from configurations with BRF=1 only. The calculated “a” parameter for the BRF=1 case is 0.3858, as can also be seen in **Figure 39**. **Table 4** shows the GSR values for BRF=1.

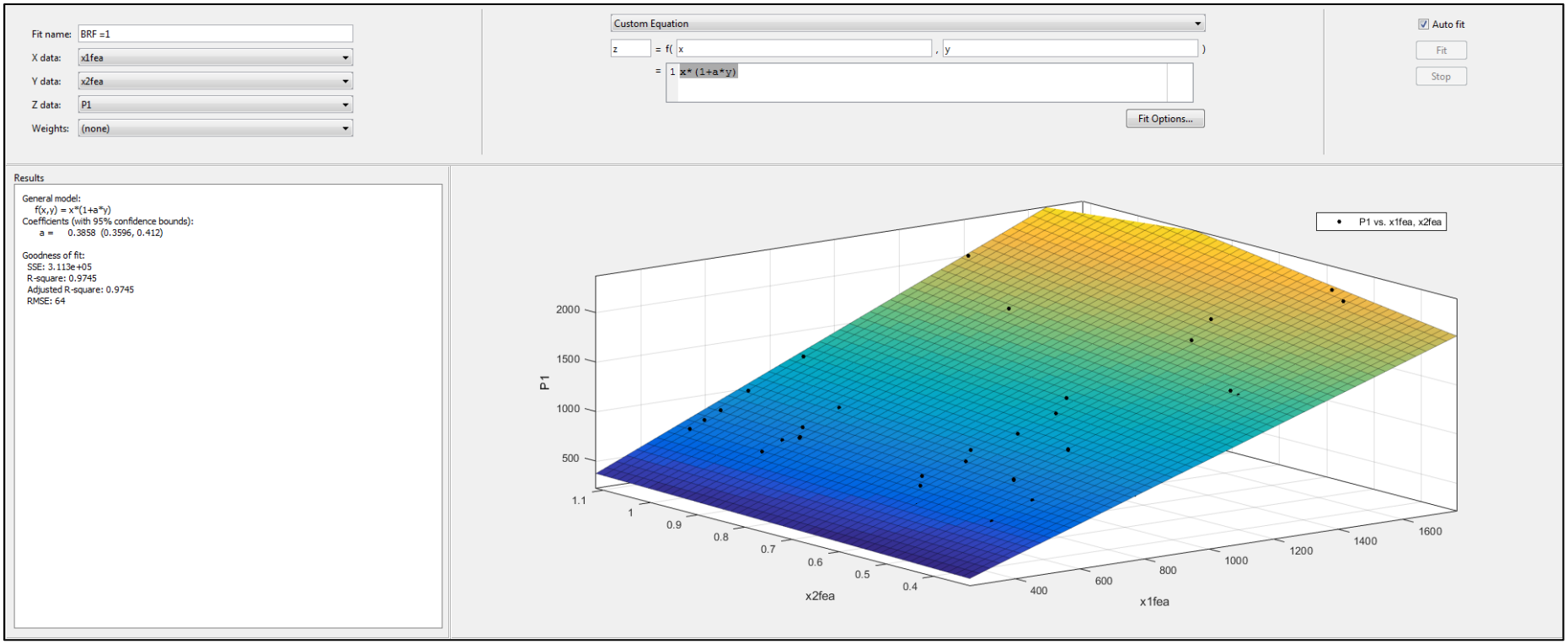

Figure 40. Fit of BRF=1 FEA results to Equation 5 to determine parameter "a"

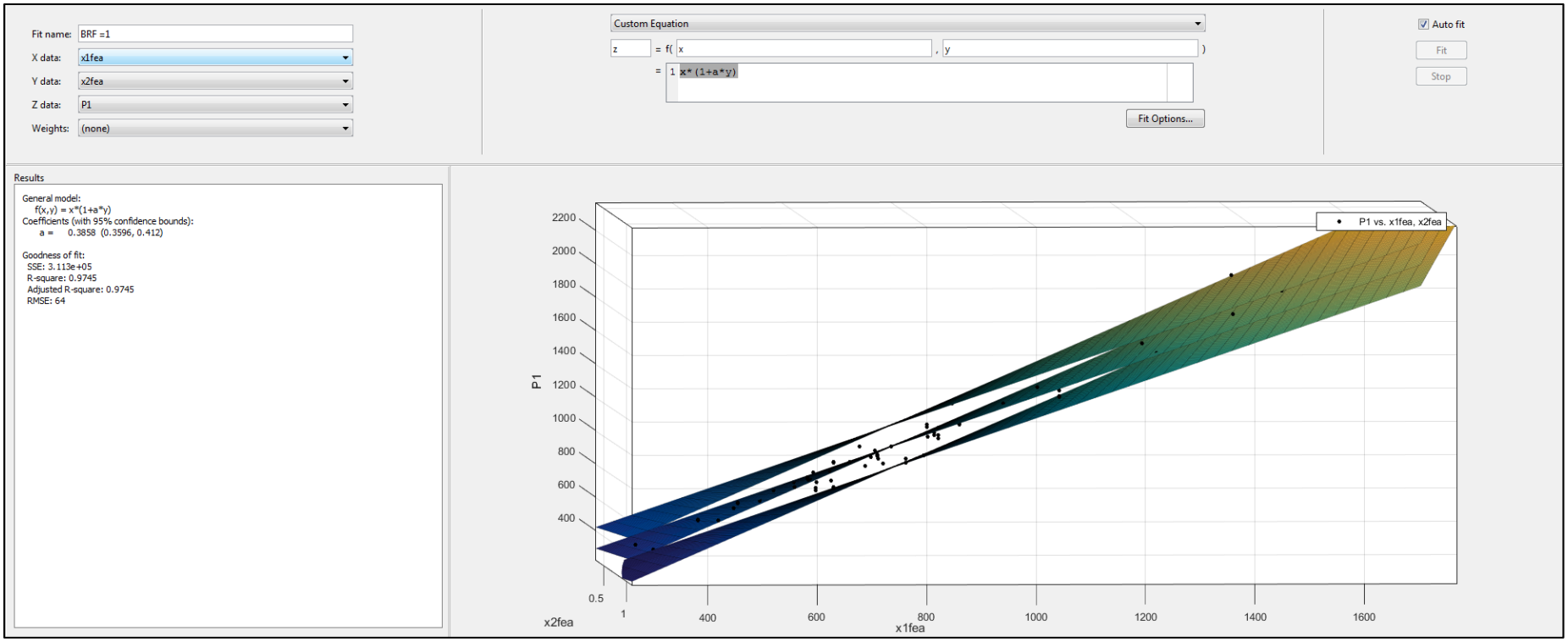

Figure 41. 95% Prediction surfaces for BRF=1 FEA model fit

Table 4. Calculated GSR values (BRF=1), a=0.3858

Pipe DR	Θ	Wall Thickness Multiplier	Geometric Strength Ratio (GSR)
7	5.625	1.0658	0.94
9	5.625	1.0760	0.93
11	5.625	1.0850	0.92
13	5.625	1.0931	0.91
15	5.625	1.1005	0.91
17	5.625	1.1075	0.90
19	5.625	1.1140	0.90
21	5.625	1.1202	0.89
26	5.625	1.1343	0.88
32.5	5.625	1.1508	0.87
7	11.250	1.1329	0.88
9	11.250	1.1535	0.87
11	11.250	1.1716	0.85
13	11.250	1.1880	0.84
15	11.250	1.2030	0.83
17	11.250	1.2171	0.82
19	11.250	1.2302	0.81
21	11.250	1.2427	0.80
26	11.250	1.2713	0.79
32.5	11.250	1.3046	0.77
7	15.000	1.1791	0.85
9	15.000	1.2067	0.83
11	15.000	1.2312	0.81
13	15.000	1.2532	0.80
15	15.000	1.2735	0.79
17	15.000	1.2924	0.77
19	15.000	1.3101	0.76
21	15.000	1.3269	0.75
26	15.000	1.3655	0.73
32.5	15.000	1.4103	0.71
7	22.500	1.2768	0.78
9	22.500	1.3196	0.76
11	22.500	1.3573	0.74
13	22.500	1.3914	0.72
15	22.500	1.4228	0.70
17	22.500	1.4520	0.69
19	22.500	1.4794	0.68
21	22.500	1.5053	0.66
26	22.500	1.5650	0.64
32.5	22.500	1.6342	0.61

Figure 42 shows the data in **Table 4**, together with the data from **Table 3**, in terms of GSR versus Pipe DR.

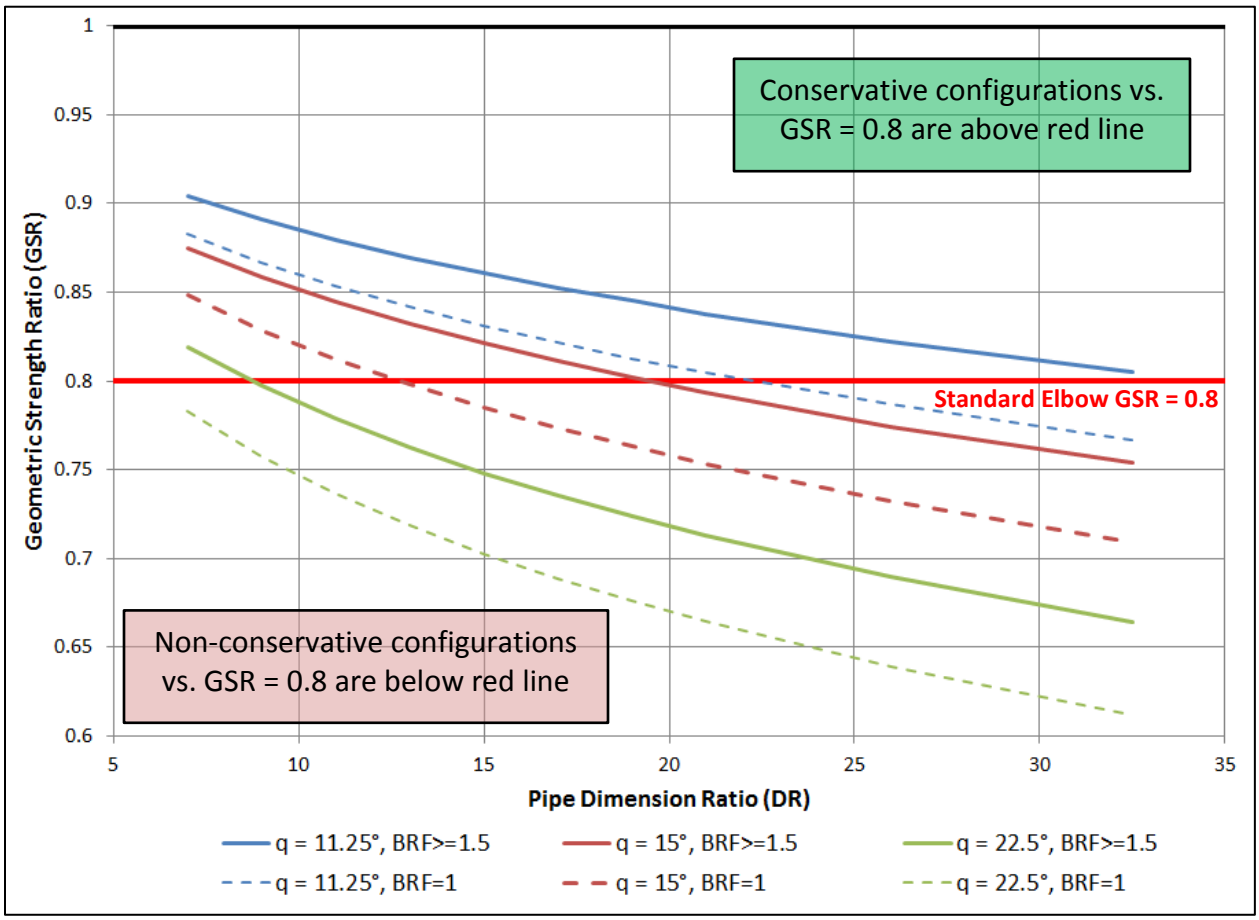

Figure 42. GSR versus Pipe DR for different miter angles, from Table 3 (BRF>=1.5) and Table 4 (BRF=1).

Figure 43 shows a comparison of the GSR values from a=0.2856 (BRF=2.5, previous work), and a=0.3858 (BRF=1) versus the updated values from a=0.3073 (BRF=1.5, 2.0, 2.5). This figure illustrates how the "a" parameter affects the calculated GSR values, higher "a" values give lower GSRs.

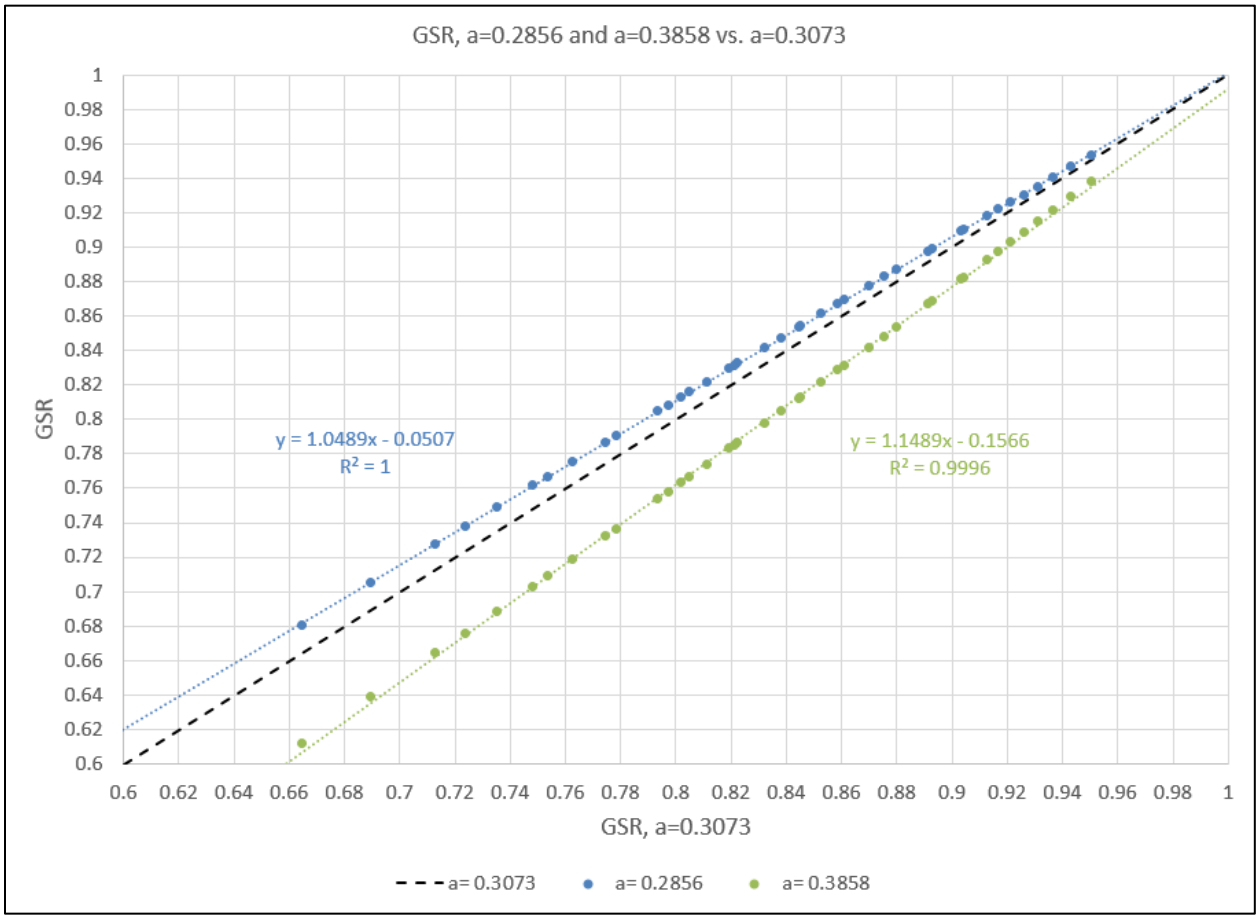

Figure 43. GSR comparison when a=0.3073 versus a=0.2856

ASME B31.3 section 304.2.3 requires the designer to address three design equations for calculating the maximum allowable pressure for a mitered elbow; equations 4a, 4b and 4c. For elbows with a miter cut less than or equal to 22.5° the lowest pressure calculated from equations 4a and 4b is specified. Equation 4c is similar in form to equation 4a and is intended for use with miter cuts greater than 22.5°. Only equation 4a has been used in this work, hence it is appropriate to briefly discuss the validity of this approach.

Figure 44 defines the geometry that the calculations reference.

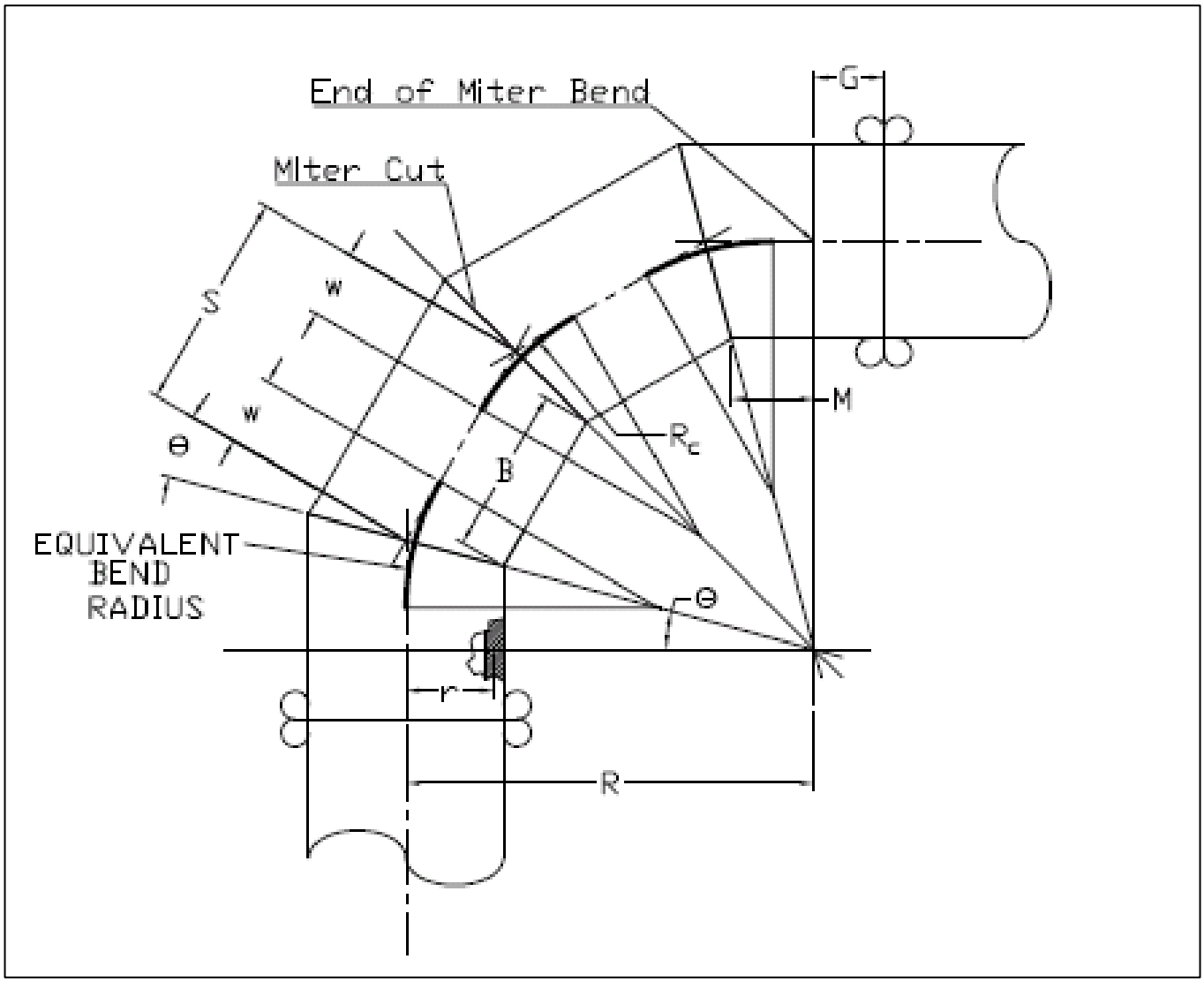

Figure 44. Mitered elbow configuration for calculations

Figure 45 shows the actual worksheet used. The actual parameter values used in these calculations are from the original work performed under GTI PROJECT NUMBER 02222-121534,

where value for “a” was calculated to be 0.2856. The value of “a” does not impact the analysis presented below as a is a linear factor in the solution.

$$R = \frac{s}{2\,\mathrm{Tan}\left[\theta \frac{\pi}{180}\right]};$$

$$P1 = \frac{S\,T}{r}\left(\frac{T}{T + a\,\mathrm{Tan}\left[\theta \frac{\pi}{180}\right]\sqrt{r\,T}}\right);$$

$$P2 = \frac{S\,T}{r}\left(\frac{R - r}{R - \frac{s}{2}}\right);$$

$$P3 = \frac{S\,T}{r}\left(\frac{T}{T + \frac{1.25}{0.643}\,a\,\mathrm{Tan}\left[\theta \frac{\pi}{180}\right]\sqrt{r\,T}}\right);$$

$$\mathrm{sol} = \mathrm{Solve}[P1 - P2 = 0,\ s]$$

$$\left\{\left\{s \to \frac{\frac{r\,T}{\sqrt{r\,T}} + 2\,a\,r\,\mathrm{Tan}\left[\frac{\pi\,\theta}{180}\right]}{a}\right\}\right\}$$

$$S = 1000;$$

$$T = \frac{OD}{DR};$$

$$r = \frac{OD - T}{2};$$

$$a = 0.2856;$$

$$s = 2.5\,OD;$$

$$OD = 14;$$

Figure 45. Equations and parameter values used in calculations

There is a point at which equations 4a and 4b are equal when:

$$s = \frac{\frac{rT}{\sqrt{rT}} + 2ar\,\mathrm{Tan}\left[\frac{\pi\theta}{180}\right]}{a} \qquad \textbf{Equation 10}$$

Evaluating **Equation 10** in the range of diameters and DR values relevant to HDPE mitered elbows shows that this occurs for very widely spaced elbows where equation 4b that is derived for a smooth torus is valid.

Figure 46 below shows that in the range of miter cut angles and DR values used in the FEA study equation 4a always provides the lower operating pressure. All three equations coincide for straight pipe.

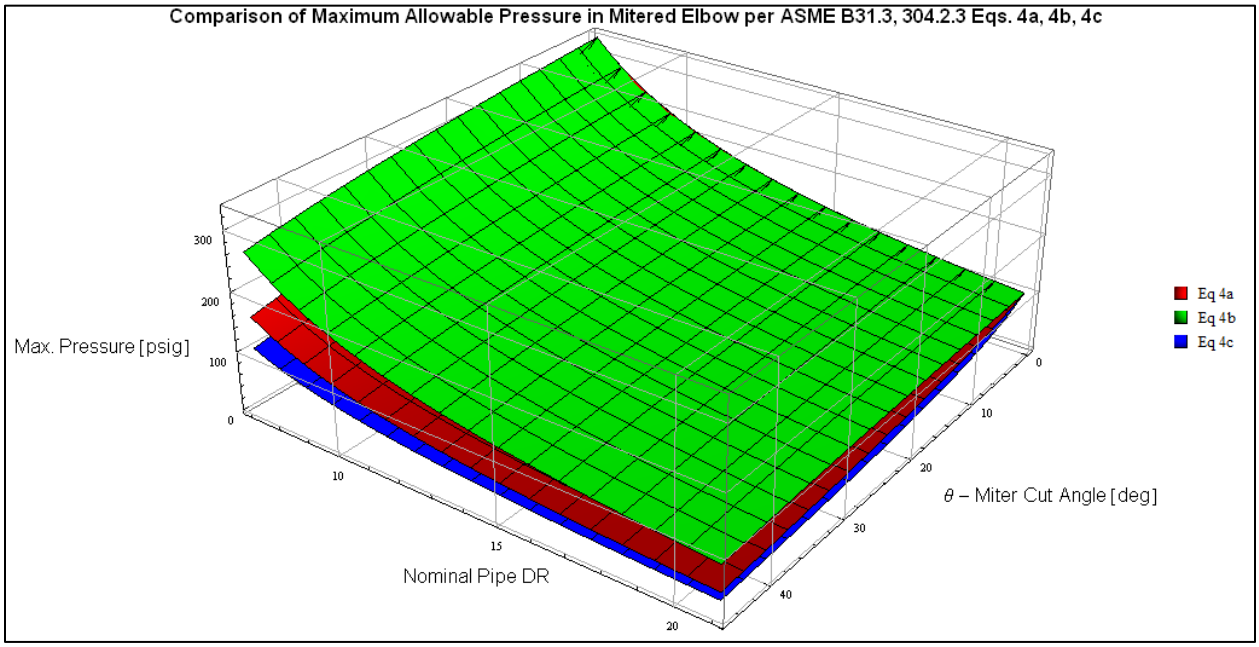

Figure 46. Comparison of ASME B31.3 elbow design equations with bend radius set to 2.5 x pipe outside diameter and a=0.643

Figure 47 and **Figure 48** show the percent difference relative to equation 4a for a=0.643 as defined in the standard and a=0.2856 as calculated in GTI PROJECT NUMBER 02222-121534. The percent difference is smaller for HDPE elbows reflecting the greater compliance of the material.

The results presented below justify the use of ASME B31.3 equation 4a (**Equation 1** in this study) as the basis for HDPE mitered elbow design and show that the analysis presented in this report will be fully consistent with ASME B31.3.

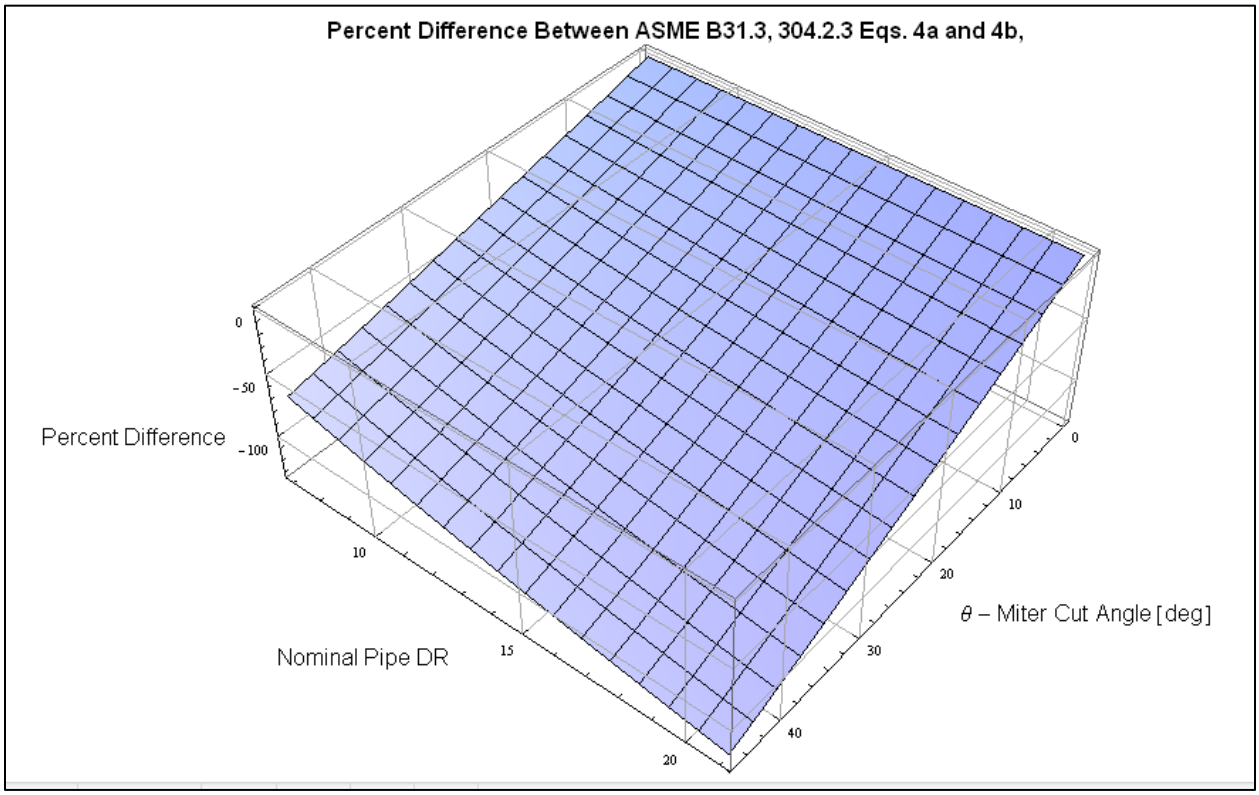

Figure 47. Percent difference between ASME B31.3, 304.2.3 equations 4a and 4b with bend radius set to 2.5 x pipe outside diameter and a=0.643 (relative to eq. 4a)

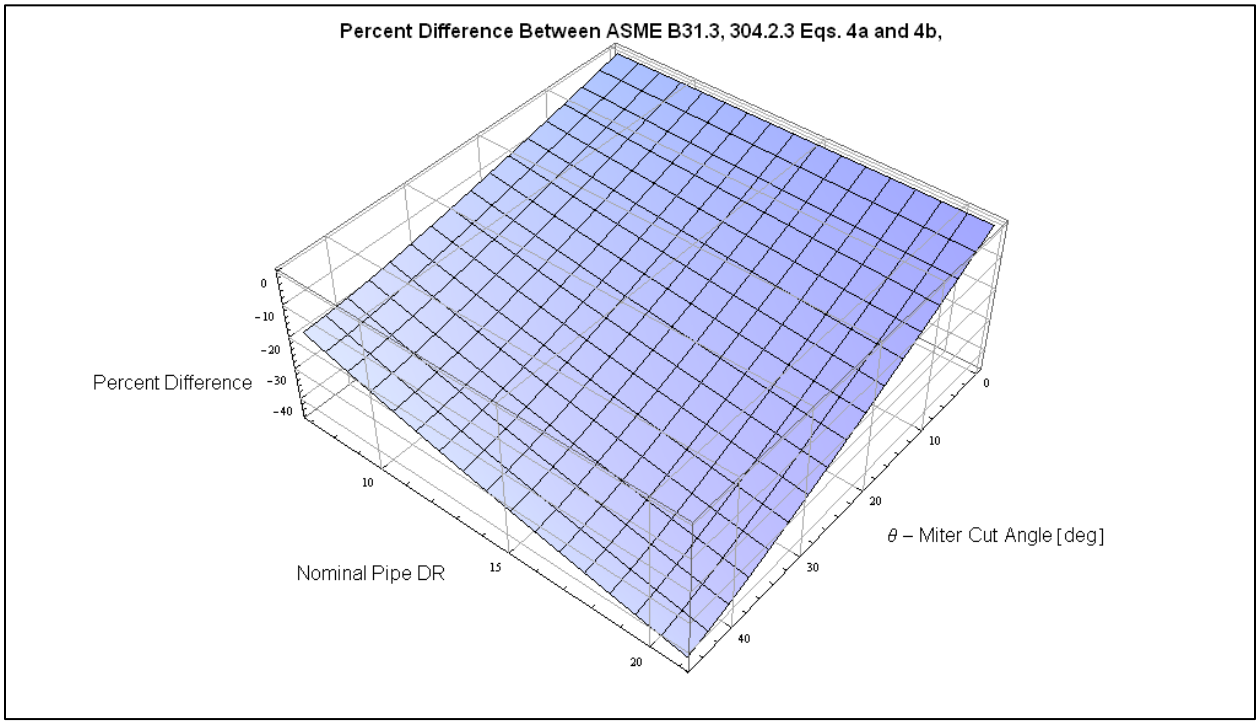

Figure 48. Percent difference between ASME B31.3, 304.2.3 equations 4a and 4b with bend radius set to 2.5 x pipe outside diameter and a=0.2856 (relative to eq. 4a)

Response Surface Evaluation

Appendices 0 – 16 provide all the necessary details to evaluate the 16 response surfaces generated in this study.

Future Work

The work done in this project has given valuable insight into the fundamental factors influencing miter bend stresses, however, the models used were simple in terms of geometry (no beads) and material model (nonlinear elastic). For further insight the following are possible in future work:

- Modeling of fusion beads
- Evaluation of thermal expansion and contraction
- Evaluation of various end constraints
- Evaluation of loading due to internal flow
- Creep analysis of various configurations
- Stress relaxation analysis of various configurations
- Expansion of the temperature range analyzed to include high temperature hydrostatic testing regimes

Bibliography

1. Green, A. and W. Emmerson, *Stresses in a pipe with a discontinuous bend.* Journal of the Mechanics and Physics of Solids, 1961. 9(2): p. 91-104.
2. Wood, J., *A study of single mitre pipe bends*. 1983, Paisley College of Technology.

END OF REPORT